AD-A230 501

Predicting the Performance
of Airborne Antennas
in the Microwave Regime

THESIS

David P. Carroll, Captain, USAF

AFIT/GE/ENG/90D-10

DTIC
S ELECTE
JAN 07 1991
E **D**

DEPARTMENT OF THE AIR FORCE

AIR UNIVERSITY

AIR FORCE INSTITUTE OF TECHNOLOGY

Wright-Patterson Air Force Base, Ohio

91 1 3 146

AFIT/GE/ENG/90D-10

Predicting the Performance
of Airborne Antennas
in the Microwave Regime

THESIS

David P. Carroll, Captain, USAF

AFIT/GE/ENG/90D-10

Approved for public release; distribution unlimited

Predicting the Performance of Airborne Antennas

in the Microwave Regime

THESIS

Presented to the Faculty of the School of Engineering

of the Air Force Institute of Technology

Air University

in Partial Fulfillment of the

Requirements for the Degree of

Master of Science in Electrical Engineering

David P. Carroll, B.S., M.S.S.M

Captain, USAF

December 1990

Approved for public release; distribution unlimited

Accession For		
NTIS GRA&I		X
DTIC TAB		
Unannounced		☐
Justification		
By		
Distribution/		
Availability Codes		
Dist	Avail and/or Special	
A-1		

Preface

Preface

The purpose of this study was to determine the capability of the Airborne Antenna Radiation Pattern Code to accurately model the performance of cavity-backed Archimedes spiral antennas mounted on or very near the fuselage of aircraft. A computer model of installed antenna performance is needed to choose the best installation locations or to anticipate deficiencies and compensate for them by other means.

A geometric model of the FB-111A aircraft was devised. A model of the cavity-backed spiral antenna's performance for vertical polarization was developed using a planar array of monopoles. The antenna model was used to simulate a spiral antenna mounted on top of the FB-111A fuselage. The predictions generated by the code were compared with measurements of an actual antenna system. The model was successful in predicting antenna patterns and as a tool for analyzing their characteristics. Differences between predicted and measured data were due to fuselage surface features near the antenna whose effects could also be missed by scale-model predictions.

My thesis advisor was Dr. Vittal Pyati. Dr. Roberto Rojas from Ohio State University ElectroScience Laboratory provided the code used in this study and guidance on its implementation. Members of the Air Force Electronic Warfare Center provided information on the antenna pattern measurements, without which this effort would have been impossible. Finally, I am owe much to my understanding wife, Pat, and my children and grandson for the time I couldn't spend with them during this thesis project.

David P. Carroll

i

Table of Contents

List of Figures

AFIT/GE/ENG/90D-10

Abstract

This study investigated the application of a high-frequency model (Uniform Geometrical Theory of Diffraction) of electromagnetic sources mounted on a curved surface of a complex structure. In particular, the purpose of the study was to determine if the model could be used to predict the radiation patterns of cavity-backed spiral antennas mounted on aircraft fuselages so that the optimum locations for the antennas could be chosen during the aircraft design phase. A review of literature revealed a good deal of work in modeling communications, navigation, identification antennas (blade monopoles and aperture slots) mounted on a wide variety of aircraft fuselages and successful validation against quarter-scale model measurements. This study developed a monopole-array model of a spiral antenna's radiation at vertical polarization and an ellipsoid-plate model of the FB-111A. Using the antenna and aircraft models, the existing Uniform Geometrical Theory of Diffraction model generated radiation patterns which agreed favorably with full-scale measured data. The study includes plots of predicted and measured radiation patterns from 2.5 to 15 Gigahertz.

PREDICTING THE PERFORMANCE

OF AIRBORNE ANTENNAS

IN THE MICROWAVE REGIME

I Introduction

1. <u>Background</u>.

a. <u>Electronic Warfare and the Radar Warning Receiver</u>. Modern military aircraft are exposed to numerous antiaircraft weapon systems and the effectiveness of combat air operations depends on the ability of aircraft to survive. Since radar is one of the primary all-weather early warning sensors for target acquisition and tracking information, proper functioning of the radar warning receiver (RWR) is vital to a mission. An RWR is an electronic warfare support measures (ESM) system that alerts the aircrew to enemy radar activity by detecting, locating, and identifying radar emanations around the aircraft (Tsui, 1986:5-7; Baron and others, 1982:59-76+). It displays a graphic picture of radar activity and presents warnings when special threat conditions (such as missile guidance activity) are present. The RWR is sometimes electroni- cally linked to electronic countermeasures (ECM) equipment (jammers and chaff and flare dispensers) to automatically initiate countermeasures

against the radar threat. Because the RWR provides both aircrew warning and hand-off threat data to active ECM systems, the RWR's satisfactory performance is essential to USAF combat operations. An RWR needs an effective antenna system to perform its vital warning and handoff functions.

    b. **Broadband Receive Antennas and the Radar Warning Receiver**. The RWR senses the electromagnetic environment through its receive antennas. RWRs typically use a small number of primary antennas (usually four) to minimize the number of components in the RWR system and to simplify the receiver's electronic circuitry. In free-space tests, cavity-backed spiral antennas closely match the performance requirements of ideal RWR antennas: high gain, wide bandwidth, and a large beamwidth. These performance requirements can be traced directly to the RWR's ESM functions.

    1) **High Gain**. The RWR should be able to detect the signal of a threat radar at a distance from the radar that allows sufficient time for aircrew warning and ECM reaction. To meet the requirement for suitable detection range, the RWR system must have sufficient signal sensitivity. The RWR antenna must therefore have high gain in its assigned region of space to meet system sensitivity requirements.

    2) **Wide Bandwidth**. Because much of the microwave portion of the electromagnetic spectrum is used by threat-associated radar systems, the ideal RWR antenna is a broadband (ideally frequency-independent) device that provides the RWR system with suitable overall sensitivity to every threat radar's emanations.

3) **Large Beamwidth**. Antiaircraft weapons can be directed at an aircraft from virtually any direction. To ensure sufficient volumetric coverage with 4 antennas, each antenna must have high gain in a full 90 degrees of azimuth and over a large range of elevation angles.

c. **Broadband Antennas and the Aircraft Structure**. As stated above, the free space antenna patterns of cavity-backed spiral antennas meet the RWR's need for wide bandwidth, high gain, and large beamwidth. The patterns of cavity-backed spiral antennas also meet the RWR's requirements when the antennas are properly installed on an aircraft at locations with an unobstructed field of view. When such is not the case, the antenna pattern will be distorted due to electromagnetic reflection and diffraction by the aircraft obstructions. To ensure the RWR can meet requirements of the aircraft's mission, the RWR system design must take into account such antenna pattern distortion. Other RWR components can compensate for some known distortion of the receive antenna patterns, but the antennas must provide reasonable gain throughout their assigned areas of coverage for the RWR to function effectively. One important requirement of RWR design, then, is to install RWR antennas at the best possible locations on the aircraft (within aerodynamic constraints).

2. **Problem**. Finding the best locations on aircraft for cavity-backed spiral antennas is an expensive, time-consuming, trial-and-error process. The existing process uses scale-model measurements, with antenna locations chosen during the final phases of aircraft design. These antenna locations are usually chosen based on aerodynamic design

considerations. Experimenting with alternate antenna locations is costly and time consuming. Scale-model measurements should be supplemented with a flexible automated method of antenna pattern modeling that can be used early in the aircraft design process.

3. <u>Summary of Current Knowledge</u>. Much success has been achieved modeling antenna patterns of communication, navigation, and identification antennas (monopole blade antennas and conformal aperture slot antennas) on a wide variety of aircraft (Kim and Burnside, 1986:554-562; Chung and Burnside, 1984:855-858; Yu and others, 1978:636-641; Marhefka and Burnside, 1976:562-565; Yu and Burnside, 1976:558-561). The Uniform Geometrical Theory of Diffraction (UTD) has been demonstrated to provide mathematical predictions of antenna patterns that are in reasonable agreement with scale-model far-field and full-scale near-field antenna pattern measurements (Burnside and others, 1985:102-245 and 1980:318-327). Computer programs have been developed and tested which apply UTD to the problem of predicting electromagnetic scattering from antennas modeled as monopoles, dipoles, aperture slots, or aperture current distributions in the presence of aircraft structures (Burnside and others, 1985:1-5: Marhefka and Burnside, 1983:2.1-2.4). The analytical basis for modeling cavity-backed spiral antennas by approximating their radiation patterns by an equivalent array of monopoles or aperture slots has been well documented (Balanis, 1982:446-522). The analytic tools necessary for this study, then, are fully developed.

4. <u>Assumptions</u>.

4

a. **High Frequency**. The model used in this study assumes the scattering shapes in the problem are much larger than the wavelength of the illuminating frequency. For the frequencies of primary interest (2 to 18 Ghz), this assumption places a lower limit (at 2 GHz) on geometric dimensions of 0.15 meters (about 6 inches). For frequencies higher than 2 GHz, the lower limit on dimensions reduces with the wavelength of the illumination. This constraint on dimensions of the scatterer allowed characterization of the basic aircraft structure.

b. **Perfectly Conducting Aircraft Structure**. The conductivity of the aircraft structure was assumed to be infinite. Composite materials were modeled as perfect conductors. Balanis and DeCarlo have demonstrated that modeling composite materials as perfect conductors yields very satisfactory results (*Balanis and DeCarlo, 1982:766-768*). Dielectric and low-conductivity portions of the aircraft (radar radome and cockpit windscreen) were modeled as "free space." Previous studies have shown that inexact modeling of the cockpit area can hamper the accuracy of predicted scattering in the region containing the cockpit (Burnside and others, 1985:165-166). This study included investigation of the inaccurate predictions caused by modeling the cockpit windscreen as "free space."

5. **Conventions Used**. This report and its discussion of electromagnetic scattering phenomena are limited to homogeneous media, with "free space" propagation assumed throughout. An $e^{(j\omega t)}$ time dependence is assumed and suppressed. The discussion centers on the electric field quantities

($\vec{E}$), but also applies to the magnetic field ($\vec{H}$) through Eq (1) (Kraus, 1984:376).

$$\vec{H} = -\frac{1}{j\omega\mu_0}\nabla\times\vec{E} \qquad (1)$$

where ω is the frequency

μ_0 is the permeability of free space

6. **Analytical Approach**. The Airborne Antenna Radiation Pattern Code (Burnside and others, 1985:1-247) was used in this study. The ability of the code to predict the characteristics of a measured radiation pattern using a geometric model of the basic structure of an aircraft and an approximate model of a cavity-backed spiral antenna was investigated. This study included development and execution of the antenna pattern model, comparison against measured data, and assessment of the modeled results.

a. **Modeling**. This study simulated the performance of 2-inch cavity-backed spiral antenna mounted on the upper starboard fuselage surface of an FB-111A (at fuselage station 311.5). The simulation consisted of a geometrical aircraft model, a planar array model of the spiral antenna, and a UTD scattering model. The aircraft and antenna models were provided as input data to the UTD scattering model contained in the Airborne Antenna Radiation Pattern Code (Burnside and others, 1985:1-247).

1) **Aircraft Model**. The aircraft (FB-111A) was modeled using a composite ellipsoid for the aircraft fuselage and flat plates for the remaining components such as wings, vertical stabilizer, and other parts. The model's composite ellipsoid dimensions were determined so the curvature of the fuselage near the antenna location closely matched the aircraft fuselage curvature. Initially, the remaining aircraft components were modeled with nine flat plates. The final aircraft model contained 11 flat plates.

2) **Antenna Model**. The cavity-backed spiral antenna was modeled as a planar array of nine electric monopoles using pattern synthesis techniques so that the model's far-field radiation pattern closely approximated the spiral antenna's actual free-space radiation. A FORTRAN-77 program for the pattern synthesis process was written for this specific purpose.

3) **UTD Model**. The default UTD model of the Airborne Antenna Radiation Pattern Code computed the geometric optics incident and reflected fields and the first-order diffraction terms. The first-order diffraction terms account for edge diffractions of the incident wave. The requirement for additional diffraction terms was made apparent when discontimuities occurred in the model output. If required, second-order diffraction terms could be included in the model output. For this study, additional diffraction terms made negligible difference in the results.

b. **Assessing the Model Results**. The computer-predicted antenna pattern data was plotted in polar format for each elevation angle. The same format was used to plot the measured antenna patterns. The predicted pattern underwent two checks: an initial review for continuity and a detailed comparison with measured data. The plots were initially screened for discontinuities and singularities. In practice, discontinuities were negligible in the patterns. Singularities in the predictions indicated that the model geometry included regions where an infinite number of rays (used to describe the directions of scattered wave components) intersect ("caustic" regions). In caustic regions, the UTD formulation could incorrectly predict infinite field strength, so other solution techniques would need to be applied. For this study, caustic regions were evident in the model plots, but were always of short angular extent. In every case, the continuous solution could be obtained by interpolating the results on either side of the caustic through the angles where the singularity occurred. When the plotted output passed screening for discontinuities and singularities, it was compared in detail to the corresponding plot of measured data.

1) **Detailed Comparison**. The plots of antenna pattern predictions from the model were overlaid on the plots of measured data to allow differences to be clearly seen. Where differences existed, the scattering geometry was closely reviewed first to determine if additional parts of the aircraft were needed in the model or if the material properties of the structure could be causing scattering effects inconsistent with those of the assumed perfectly conducting structure. When

8

differences between the predicted and measured patterns could not be explained by inaccuracies in the aircraft model, the prediction error was highlighted for later review. The unexplained inaccuracies for several elevation angles and illumination frequencies were compiled. The compiled data could be used to indicate trends in the prediction errors so that the inaccurately-modeled scattering mechanisms could be identified. Results of the detailed comparisons include a summary of the model's accuracy and inaccuracy in predicting the actual antenna performance.

7. **Materials and Equipment**.

a. **Computer Resources**. The Airborne Antenna Radiation Pattern Code was run on the AFIT Hercules Digital Equipment Corporation VAX 11-785 computer. The latest executable version of this code was obtained from the Ohio State University ElectroScience Laboratory, installed on the computer, compiled, and verified as operational using input data and results documented in the code's user manual.

b. **Measured Antenna Patterns**. The Air Force Electronic Warfare Center (AFEWC, the thesis sponsor) provided the measured FB-111A antenna pattern data used in this study.

8. **Document Organization**. The remainder of this document is organized as follows.

a. Chapter II is a detailed review of literature documenting previous work in predicting airborne antenna patterns.

b. Chapter III describes the methodology followed in applying the Uniform Geometrical Theory of Diffraction to predicting the radiation pattern of the cavity-backed spiral antenna mounted on the FB-111A fuselage.

c. Chapter IV contains results and discussion of the antenna pattern modeling.

d. Chapter V provides conclusions and recommendations for further research.

II Literature Review

1. **Introduction**. This chapter reviews prior experimental and analyti-
cal work in predicting the radiation patterns of airborne antenna
systems at microwave frequencies (typically 300 Mhz to 100 GHz) (Skol-
nik, 1980:7) and defines the extension of that work accomplished in this
study. Transmitting and receiving airborne electronic systems are
highly dependent on the performance of the antenna systems that inter-
face them with the electromagnetic environment surrounding the aircraft
(Kraus, 1990:Ch 3, 3-9). Much work has been done in analyzing and
designing individual antenna components to achieve desired radiation
patterns in free space. Significant work has also been accomplished in
analyzing and verifying the performance of certain classes of antennas
in the presence of obstructions having various mounting geometries.
This chapter contains, first, a description of how predicting aircraft
antenna patterns has evolved into an automated computational process.
Next, a review is made of work done to date in applying mathematical
predictions to the performance of two important classes of antennas
(monopole blades and aperture slots) on a variety of aircraft types. A
description is presented of how aircraft are geometrically modeled so
that existing diffraction theories can be applied to airborne antenna
pattern studies. The chapter ends with a definition of how this study
extends the prior application of high-frequency scattering techniques to
aircraft antenna pattern prediction.

2. **Evolution of Antenna Pattern Prediction**. The science of locating antennas on aircraft has evolved over the years from a "seat-of-the-pants" operation to a maturing application of increasingly powerful computational techniques.

    a. **Early Developments**. Since World War II, electronic transmitting and receiving systems (including radios, radars, direction-finding equipment, navigation aids, identification transponders, and electronic warfare systems) have become increasingly important to aircraft mission and survival. Engineers recognized as early as 1948 that antenna system radiation pattern prediction was essentially a specialized electromagnetic scattering problem (Kim and Burnside, 1986:554). Before the 1960s, mathematically predicting antenna radiation patterns could be achieved by modal analysis of the boundary conditions imposed by the electromagnetic scattering mechanisms present. Due to the complexity of mathematical reduction and numeric computations involved in modal analysis, investigations were limited to simple shapes (such as single antennas on infinitely long circular and elliptic cylinders) (Burnside and others, 1973:780-781). The insightful application of well-established techniques used in the field of optics significantly simplified the mathematical operations and computations required to analyze complex microwave antenna pattern problems.

    b. **The Geometrical Theory of Diffraction**. In the early 1960s, James Keller demonstrated, with his Geometrical Theory of Diffraction (GTD), that certain electromagnetic scattering phenomena could be very closely approximated using relatively simple ray propagation principles

from the field of optics (Keller, 1962:116-130). For scattering

problems in which the frequency of the electromagnetic radiation was

high enough (that is, the electromagnetic wavelength was much smaller

than the physical size of the scattering object) GTD offered a simpli-

fied problem formulation that was reasonably accurate at most locations

around the scatterer. The GTD formulation treated scattering from a

complex shape as the superposition of contributions from various

"scattering centers" on the complex shape. Using GTD, the geometry of

each scattering center could be treated as a separate scattering problem

and solutions to many canonical shapes (spheres, cylinders, cones, and

other basic geometric solids) could be individually obtained and used to

reconstruct the scattering from complex conducting bodies. GTD predicts

infinite fields at shadow boundaries where the GO incident or reflected

fields stop abruptly. Despite GTD's limitations, it proved to be a

powerful tool in predicting antenna radiation patterns for some geome-

tries (Burnside and others, 1973:780-786). Today, correction coeffi-

cients and other refinements have been applied to the basic GTD tech-

nique to overcome many of its limitations.

c. **The Uniform Geometrical Theory of Diffraction (UTD)**. The

difficulties GTD had in predicting fields in the transition regions were

addressed in the development of the Uniform Geometrical Theory of

Diffraction (UTD) (Kouyoumjian and Pathak, 1974:1448-1461). UTD retains

the GTD formulation (superposition of scattered fields from small

scattering centers). UTD accounts for the GTD limitations by introduc-

ing transition functions that eliminate GTD's singularities at the

shadow boundaries, hence providing a uniform solution. Since the mid-

13

1970s, the increasing power and availability of digital computers and the development of efficient UTD computation algorithms allow UTD to be used as a practical method of numerically analyzing high-frequency electromagnetic scattering problems. Since UTD's inception, it has been applied to antenna radiation problems and has been verified (Burnside and others, 1985:89-245, Marhefka and Burnside, 1983:7.9-7.18, Pathak and others, 1981:617-620; Balanis, 1989:819-823) as an accurate approximation to high frequency scattering. UTD's high frequency assumption places a lower limit on the dimensions of the scattering object, but this limit can be relaxed under certain conditions (Yu and Burnside, 1976:559). Further work (Balanis and DeCarlo, 1982:766-768) demonstrated that UTD analysis based on assumed perfectly conducting obstructions achieved accurate predictions of scattering by composite materials with conductivities as low as 10^4 Siemens/meter. Figure 1 illustrates how closely UTD predictions compare to measured experimental data. One known limitation of UTD is its failure to accurately predict scattered fields in caustic regions. In caustic regions, other solutions must be applied. Fortunately, the steps involved in UTD computations accurately predict the locations of caustic regions, and other solution techniques can be applied there. In many instances, the caustic region is so small that the continuous behavior of radiation in the caustic region can be found by simply interpolating the valid UTD results just outside the caustic region. In other cases, UTD results can be combined with other approximation methods to obtain acceptable results everywhere. UTD, then, can be accurately applied to microwave electromagnetic radiation problems involving antennas in the presence of complex shapes and materials characteristic of aircraft.
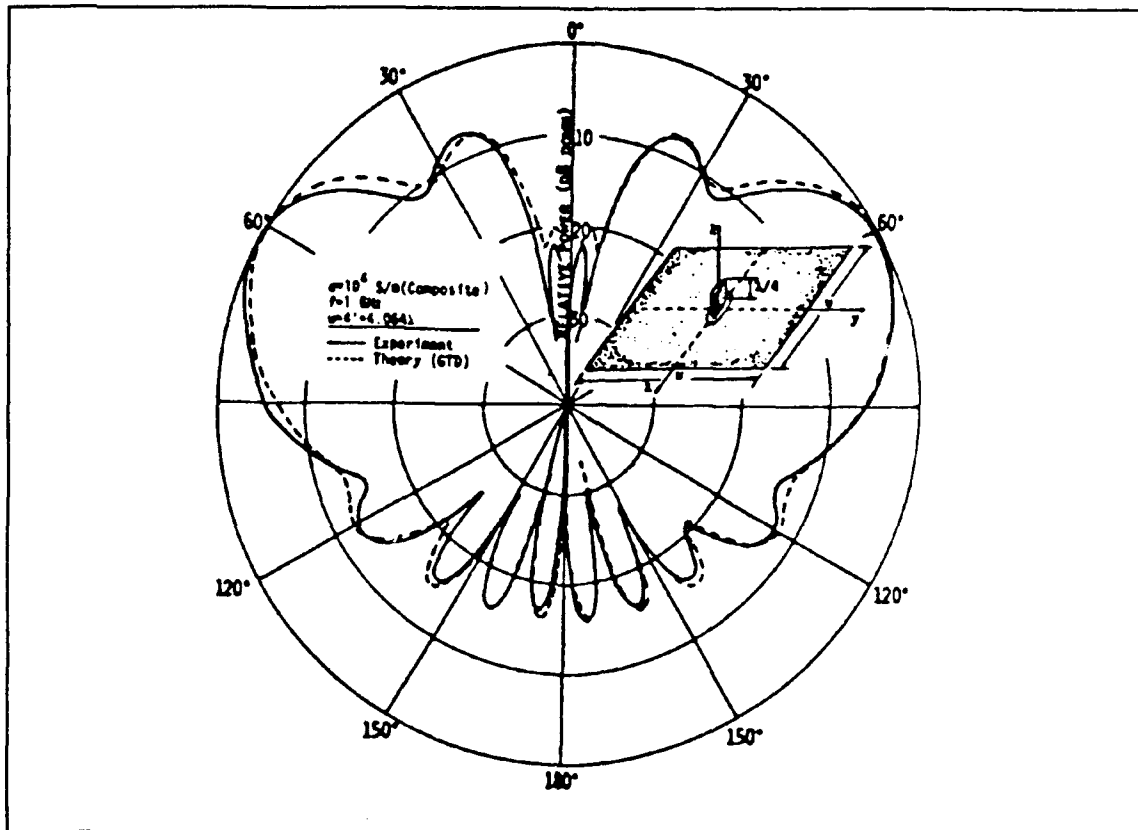
Figure 1. Elevation Plane Amplitude Patterns of a λ/4 Communication, Navigation, Identification Monopole Antenna Above a Square Composite Ground Plate (Balanis and DeCarlo, 1982:768)

3. **Applying Electromagnetic Scattering Analysis to Predicting Antenna System Performance**. Application of GTD and UTD to antenna pattern prediction has evolved from investigating the effects of a simple scatterer in an antenna's field of view (Howell, 1975:46-49) through various applications of the theory to more complex scattering problems (Fahmy and Botros, 1979:615-624; Marhefka and Burnside, 1976:562-565). Antenna pattern studies have been sponsored by the Navy, Air Force, and NASA for aircraft ranging from the Boeing 747 to the F-16, and for the Space Shuttle. The literature contains a simplified algorithm for

formulating antenna radiation pattern problems and applying UTD to their solution (Kim and Burnside, 1986:554-556 and Veruttipong, 1984:35-38). Today several computer programs are based on UTD (Kim and Burnside, 1986:554-562; Burnside and others, 1985:14-37; Marhefka and Burnside, 1983:2.1-2.4; Cooke and Ryan, 1980:631-634) whose predictions have proved accurate for monopole and conformal slot antennas mounted on aircraft fuselages and the upper surfaces of aircraft wings (Marhefka and Burnside, 1976:562-565). The computer programs can be used for other antenna types provided the characteristics of the antenna can be modeled as combinations of monopoles and slots or in terms of current distributions along the aircraft's surface. The UTD results have been verified by comparing them against actual field measurements of scale-model aircraft antenna systems in the far-field (location of observation is several wavelengths away from the antenna) (Yu and others, 1978:636-641; Yu and Burnside 1976:558-561) and to measurements of full-sized antenna patterns in the near-field (location of observation is within a few wavelengths of the antenna) (Burnside and others, 1980:318-327). Figure 2 shows how well UTD predictions agree with measured data. The data in Figure 2 is from a 1/4 scale model.

4. **Modeling Aircraft Structures Using Basic Geometric Shapes**. The computer programs for predicting aircraft antenna radiation patterns via UTD have used an assortment of shapes to describe the aircraft structure. Specialized work in modeling the interaction of a monopole antenna on a finite curved ground plane requires an accurate description of the curvature of the fuselage segment that forms the ground plane. Several geometric shapes have been used to model fuselage shapes: right
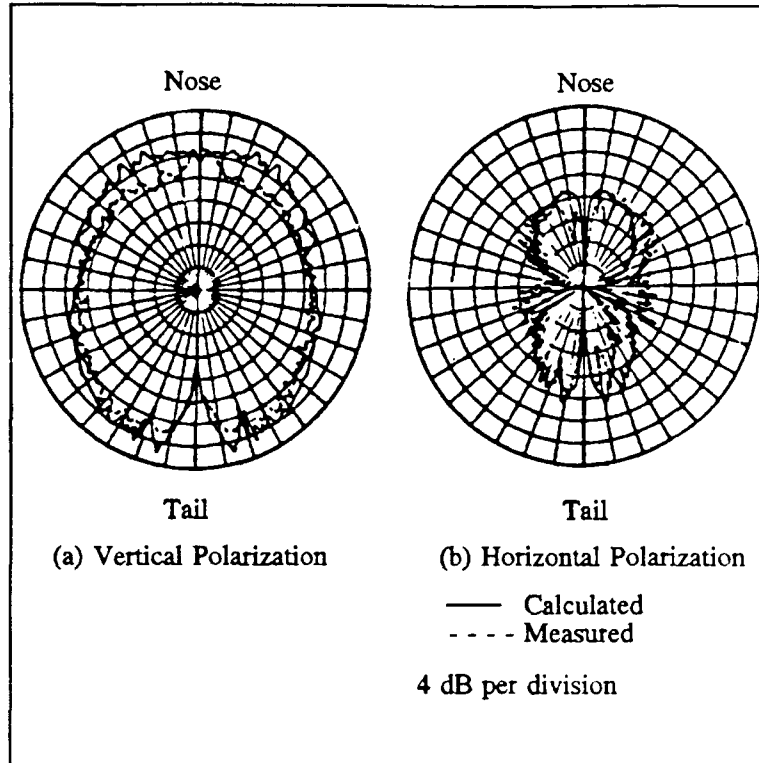
Figure 2.   Elevation Plane Amplitude Patterns
for a TACAN Antenna Mounted on Top
of an F-16 Fighter Aircraft (Burn-
side and others, 1985:182)

circular cylinders and cones (Fahmy and Botros, 1979:615-624), prolate
spheroids (solid geometric bodies with circular axial cross-sections and
elliptic longitudinal cross-sections having eccentricity greater than 1)
(Yu and Burnside, 1976:558-561; Chung and Burnside, 1984:855-858), and
composite ellipsoids (solid geometric bodies with ellipti axial and
longitudinal cross-sections) (Kim and Burnside, 1976:554-562). Accu-
rately modeling the fuselage curvature is critical to determining the
fuselage's effects as a ground plane, and is also necessary for accu-
rately describing the diffraction of electromagnetic energy around the
surface of a curved structure removed from the antenna mounting location

(the "creeping wave") (Burnside and others, 1980:318-321). Aircraft

wings, horizontal and vertical stabilizers, and other flat structures

are modeled using flat or bent conducting plates systematically connect-

ed to the fuselage and each other as necessary to depict the aircraft

(Burnside and others, 1985:38-41; Yu and others, 1978:636-639).

Typically, the aircraft nose radome is modeled as "free space" (the

fuselage is chopped off abruptly where the radome begins) to represent

the predominantly dielectric (electromagnetically transparent) nature of

radome material. Using the combination of a fuselage and multiple

plates, models of commercial airliners, military transport and fighter

aircraft, and small private airplanes have been constructed in the

course of antenna radiation pattern studies. The cockpit areas of

fighter and small private aircraft have presented problems for analysts

because of the complexity of materials and structures present (Chung and

Burnside, 1984:855-858). The example mathematical aircraft model in

Figure 3 (a 12 plate model of the F-16 used to calculate the predicted

data in Figure 2) demonstrates that a simple aircraft model can be used

to achieve very useful antenna performance predictions. Specific tech-

niques for modeling aircraft are detailed in two references (Burnside

and others, 1985:15-35; Yu and others, 1978:636-639).

5. **How This Study Extends the Existing Published Knowledge**. This study

develops a model of the cavity-backed spiral antenna that is compatible

with the Airborne Antenna Radiation Pattern Code, compares predicted

antenna patterns with full-scale far-field measured data and discusses

differences between observed and predicted phenomena, demonstrates the

effects of variations in aircraft model dimensions on predicted antenna

(a) Actual Side View   (b) Model Side View

(c) Actual Front View   (d) Model Front View

(e) Actual Top View   (f) Model Top View
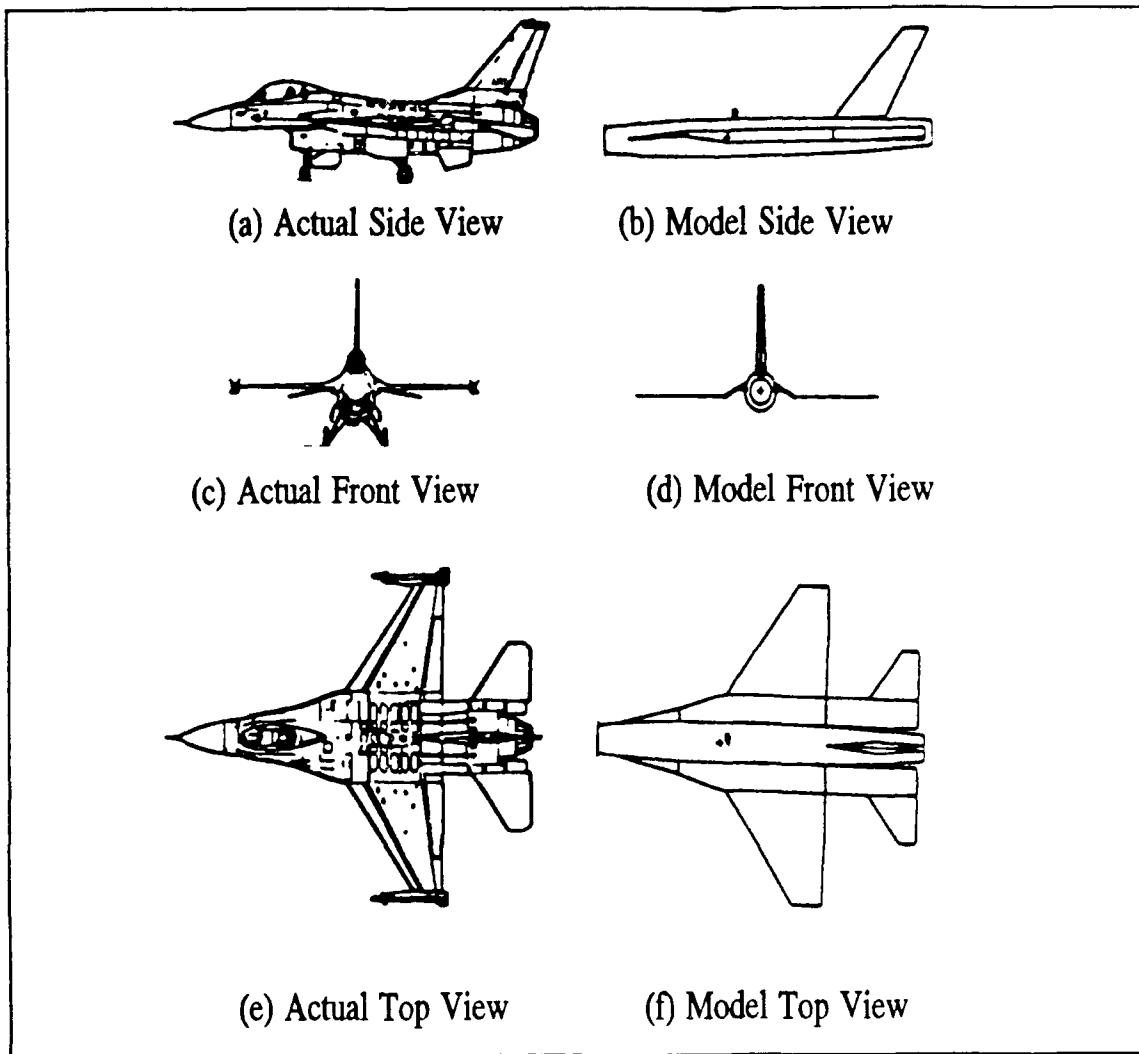
Figure 3. F-16: Actual and Geometric Model (Burnside and others, 1985:168)

patterns, and suggests methods to improve the UTD prediction of antenna radiation patterns using other scattering models.

III Methodology

1. **Introduction**. This chapter contains an explanation of how the
Uniform Geometrical Theory of Diffraction (UTD) applies to the electro-
magnetic scattering problem represented by microwave antennas mounted on
aircraft. The chapter begins with a description of UTD's basic problem
formulation, then summarizes the processing performed by the Airborne
Antenna Radiation Pattern Code in applying UTD to antenna pattern
prediction. Next the development of models of the aircraft and antenna
is described. Finally, there is a short discussion of the software used
in performing the study.

2. **The Uniform Geometrical Theory of Diffraction**. UTD (Kouyoumjian and
Pathak, 1974:1448-1461) is an enhancement of the earlier Geometrical
Theory of Diffraction (GTD) (Keller, 1962:116-130). Both GTD and UTD
are based on and extend Geometric Optics (GO), a high frequency scatter-
ing solution (Kline and Kay, 1965:10). These high frequency techniques
are based on ray-tracing and assume diffraction, like reflection, to be
a highly localized phenomenon. UTD breaks a complex scattering shape
into a number of smaller objects (called scattering centers) with
simpler shapes. The fields due to all scattering centers on an object
are solved, then those fields are superimposed to obtain the total field
at an observation point. The UTD formulation for the scattering problem
is illustrated (for the two-dimensional case) in Figure 4. The field at
the observation point consists of the direct field (straight from the
source to the observer), the reflected field (simply reflected from the

20
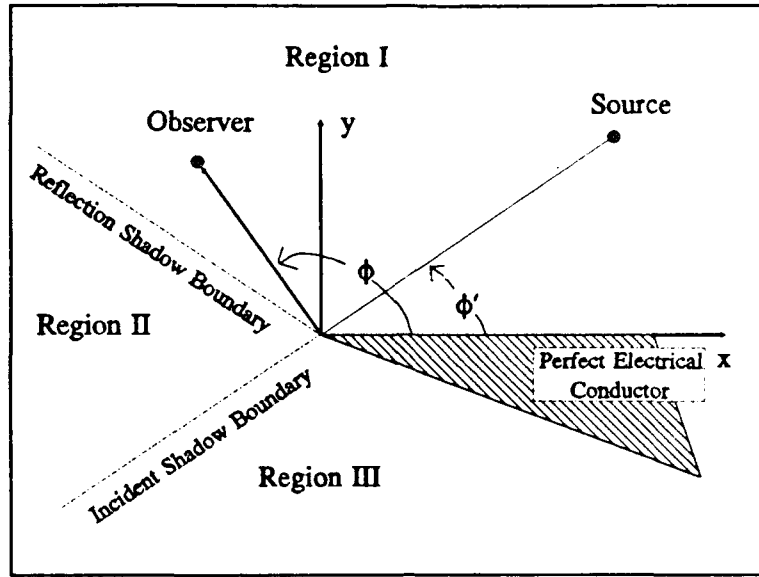
Figure 4.   Geometry for UTD Formulation

object surface to the observer), and the diffracted field(s) due to
discontinuities on the object surface. By applying basic principles to
the scattering case in Figure 4, it can be seen that not all fields
exist in all regions. The direct field cannot exist in Region III be-
cause the field cannot propagate through the perfect conductor. The
reflected field can only exist in Region I, because the reflection
shadow boundary forms the largest angle ϕ for which Snell's law of
reflections is satisfied. The shadow boundaries define the limits to
the regions in which the direct and reflected fields can exist. The
direct and reflected field parameters are found using GO techniques.
The diffracted field is computed by first determining the incident field
at the point of diffraction, then computing UTD's diffraction coeffi-
cients (with appropriate angle and distance arguments describing the
observation point) and multiplying the incident field by them to
determine the diffracted field at the observation point. The total

field at the observer is the sum of the GO direct and reflected fields plus the superposition of all diffracted fields from the scattering centers on the complex shape. Many references detail UTD's development and implementation (Balanis, 1989:743-835; Pathak,1988; Ch 4, 1-115; Kouyoumjian and Pathak, 1974:1448-1461). Computations necessary to determine UTD's terms and the ray trajectories for the various field components making up the total scattered field have been programmed in efficient computer codes (Burnside and others, 1985:1-7; Marhefka and Burnside, 1983:Ch 1,1; Cooke and Ryan, 1980:631-634). The Airborne Antenna Radiation Pattern Code (Burnside and others, 1985:1-7) is designed specifically to solve problems involving sources on a curved aircraft fuselage.

3. **Application of the Uniform Geometrical Theory of Diffraction to Airborne Antenna Pattern Prediction**. The Airborne Antenna Radiation Pattern Code implements an efficient UTD model. The model's basic scattering shapes include the composite ellipsoid (fuselage) and various wedges made up of flat plates. UTD solutions for the composite ellipsoid and wedge shapes have been well-documented and verified through comparison with measured results (Burnside and Marhefka, 1988:20.62-20.97; Burnside and others, 1985:74-246; Marhefka and Burnside, 1983:Ch 7; Pathak and others, 1981:609-622). The Airborne Antenna Radiation Pattern Code computes the total UTD field at an observation point by systematically determining various ray paths and the source field parameters contributing to fields along the paths (Burnside and others, 1985:1-11).

a. **Direct Fields**. The UTD technique for determining the far-field
radiation pattern of an antenna on a curved surface first involves
determining the path from the source to observer. For points separated
by free space, the path is a straight line. If an object lies between
the two points, the geodesic must be determined. A "geodesic" is the
path of shortest propagation time between two points on a surface. If
the path of shortest time along the surface of the intervening object
traverses a discontinuity on the surface, localized diffraction takes
place at the discontinuity and UTD determines the diffracted field as
discussed below. If the geodesic traverses only continuously curved
surfaces of the intervening object, surface diffraction takes place, and
the geodesic path is computed to obtain the correct surface diffraction
field at the observer. If a direct free-space path exists, geodesic
paths are ignored, since the contribution of fields taking such paths is
assumed to be insignificant when compared to the direct field.

b. **Reflected Fields**. Next, paths for reflection of the source's
direct field to the observer are determined. In this code, computation
of reflection paths is facilitated by the convention used for defining
the corners of conducting plates. Plate corner locations are entered in
a counter-clockwise order when the plate is viewed from a vantage point
on the side of the plate illuminated by the source.

c. **Diffracted Fields**. Once direct, surface-diffracted, and
reflected fields have been identified, diffraction of the direct source
field by the scatterer is computed. Additional terms (diffraction of
reflected fields, reflection of diffracted fields, and double reflec-

tions and diffractions) are computed last (if specified by the user in the input data).

d. **Calculation of Power Pattern Value**. Once the paths are known, appropriate GO, GTD, and UTD equations are applied to obtain the polarization, amplitude, and phase of each field component contributing to the field at the observation point. All fields existing at the observation point are then coherently summed. The resultant field is then decomposed into two convenient orthogonal components, and the magnitude of each is squared to obtain the power density at the observation point. For this study, observation points were chosen in the far field of the antenna under study. Each point was defined by the polar angles θ and ϕ in the direction of the observation point in the pattern plot coordinate system (described below) (Burnside and Marhefka, 1988:Ch 20,7-37). In this study, power patterns were calculated in one degree increments for ϕ ranging from 0° to 360°. The resultant dataset was then normalized by dividing the absolute value of the field magnitude at each observation point by the highest field value in the entire range of ϕ for the fixed elevation angle (θ). Generally, this resulted in a modeled power pattern approximately 4 dB below that of a measured power pattern, since the cavity-backed spiral antenna's maximum gain was typically 4 dB at the frequencies analyzed. Values of measured data were also scaled so the peak gain at a fixed elevation angle was unity. Plots of predicted and measured radiation patterns were made on the same axes and scales. Once the predicted and measured data were normalized to a maximum of unity, the plots were a fair representation of the shape of the radiation pattern, but did not necessarily represent actual abso-

24

lute values of the antenna system gain. Normalizing the measured and predicted data using total radiated power was considered. However, unlike a free-space antenna pattern, the power in the system is not distributed uniformly in space. Normalization to unity maximum gain provided a convenient scale for plotting and at least subjective analysis. In this report, the normalized model and measured power patterns are plotted in polar format with units of decibels referenced to an isotropic source (dB_i).

4. **Aircraft Model**. This study involved an analysis of the measurements of the generic F/FB-111 to develop a baseline model of the aircraft's scattering properties in the principal azimuth plane (0° elevation in the coordinate system shown in Figure 5). The baseline model was then
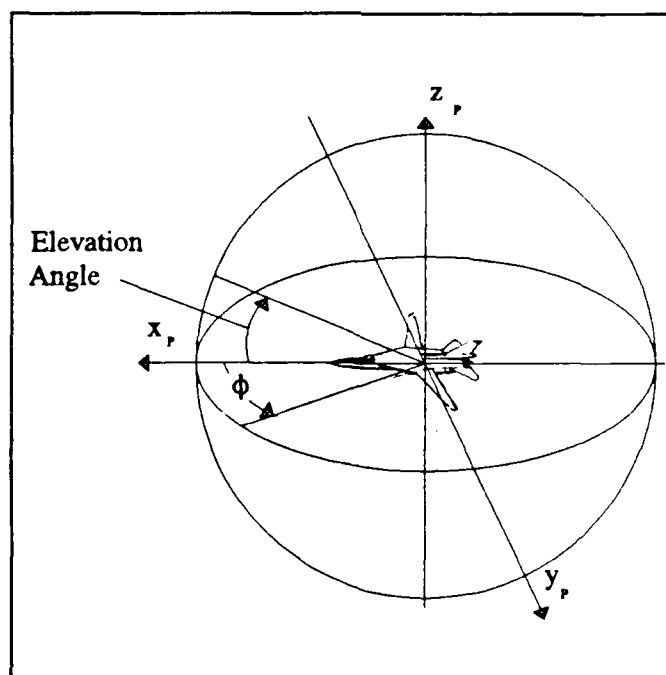
Figure 5.   Pattern Plot Coordinate System

improved by increasing its detail to a point where it could successfully represent the actual aircraft's scattering effects over a 40° range of elevation angles (20° to −20°). The aircraft used for the antenna pattern measurements was the Rome Air Development Center's full-size FB-111A airframe with wings swept to 40°.

a. **Baseline Model**. Modeling the aircraft structure requires both an accurate interpretation of the aircraft's physical dimensions and insight into the electromagnetic scattering process. Modeling the FB-111A structure was facilitated by directly using the aircraft Fuselage Station, Buttock Line, and Water Line numbers, which are referenced in inches, to find the dimensions of the aircraft model plates and ellipsoids. Fuselage Station (FS) numbers start near the tip of the nose (FS 0) and extend aft down the axis of the fuselage. Buttock Line (BL) numbers start at the axis of the fuselage (BL 0) and extend radially out from the fuselage axis. Water Line (WL) numbers locate planes parallel to the aircraft horizontal vision plane and are referenced to the lowest portion of the aircraft fuselage (WL 137). Adhering to the conventions in the Airborne Antenna Radiation Pattern Code User's Manual, the aircraft model was developed so its fuselage axis was the z-axis, with the nose directed in the negative z direction. The wings lay in the y-z plane, and positive x direction pointed up from the fuselage axis to the top of the fuselage. With these conventions, the starboard (right) half of the aircraft was defined as the half-space y < 0 as shown in Figure 6. Model development consisted of determining the fuselage curvature near the antenna mounting location, choosing locations to chop

26

the fuselage to model changes in material, and selecting flat plates to accurately represent the scattering properties of the aircraft.
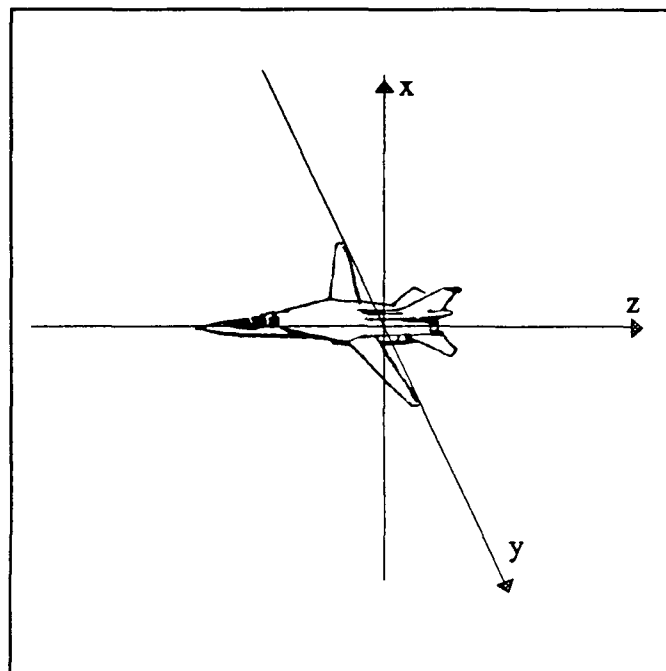
Figure 6.   Aircraft Model Coordinate
             System

1) __Fuselage Curvature Near the Antenna__. The scattering code models the fuselage as a composite ellipsoid consisting of two semi-ellipsoids whose major axes lie on the z axis: one extending from the origin in the positive z direction, and the other extending from the origin in the negative z direction. The two semi-ellipsoids join in the x-y plane so their cross-sections are identical ellipses, resulting in a smooth, continuous surface at the intersection. The cross-sectional ellipse dimensions can be determined by examining aircraft drawings or scaled photographs having a cross-sectional view near the antenna

mounting location. For the FB-111A antenna problem in this report, an exact cross-section was available for the fuselage station at the antenna mounting location (Miller, 1982:76). The cross-section at this fuselage station (FS 311.5) was chosen to be the x-y plane for the aircraft model. The parameters for the cross-sectional ellipse were determined by directly measuring the one-hundredth scale drawing of this cross-section. The centroid of this cross-sectional ellipse became the aircraft model origin. The dimensions of the semi-ellipsoids in the positive and negative z directions were determined by measuring the waterline displacement of the fuselage surface (x dimension) at a fuselage station (z dimension) away from the model origin and substituting these values into the Eq (2) (describing an ellipse on the z-x plane) to determine the model ellipsoid parameters (Salas and Hille, 1974:367).

$$\frac{z^2}{a^2} + \frac{x^2}{b^2} = 1 \tag{2}$$

where a and b are as depicted in Figure 7. A similar computation was made to establish the ellipsoid dimensions in the y-z plane.

2) **Determining Fuselage Chop Locations**. Determining which material interfaces (radar radome, cockpit windscreen, or other abrupt change in fuselage material both fore and aft of the antenna location) dominate the response of the antenna necessitated making assumptions about the material properties of the radome and windscreen material. Since the windscreen (assumed to be dielectric) was much nearer the

28
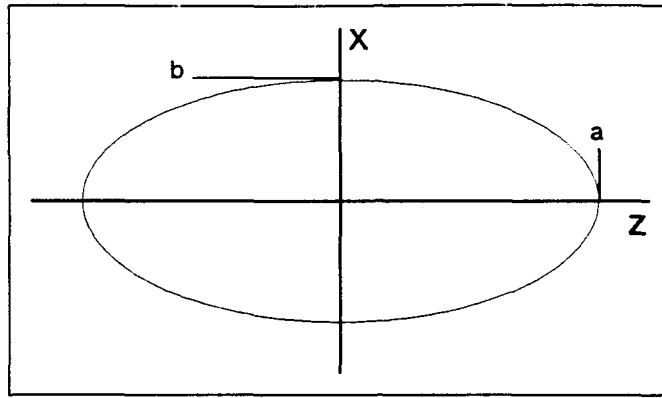
Figure 7. Ellipse Parameters

antenna mounting location than the radar radome, the fuselage was initially chopped at the cockpit rear bulkhead (FS 278.5).

3) <u>Modeling Scattering Shapes Using Flat Plates</u>. Aircraft components other than the fuselage were modeled as shapes made up from flat plates. Each plate was entered into the scattering code by specifying the locations of each corner. Corner locations were obtained from the three-view drawings in the Technical Order (Department of the Air Force, 1988:Ch 1,5) and referenced to the model coordinate system. The model allows each plate to have up to six corners. Corner locations were entered in a specified order so they defined the plate edges in a counter-clockwise ("right hand") sense when viewed from the side of the plate upon which the source was incident. To ensure plates were flat, the relationship shown in Eq (3) was used to ensure each corner point (x_i, y_i, z_i) lay on a common plane described by constant coefficients A, B, C, and D (Salas and Hille, 1974:591).

29

$$Ax_i + By_i + Cz_i + D = 0 \qquad (3)$$

The precision and detail required in modeling aircraft components should increase with the components' proximity to the antenna, because objects closer to the antenna will have more influence on its radiation pattern. Modeling the curvature of components near the antenna (such as the leading edge of the wing glove) involved trading off precision for model complexity. The sensitivity of the model prediction to different profiles for the wing glove leading edge shape was determined by iteratively executing the scattering model with various flat plates representing the actual (curved) surfaces (the results are discussed in Chapter IV). At significant distances from the antenna (such as the vertical stabilizer), very simple geometry could be used in modeling the aircraft. Aircraft components outside the antenna's viewing angle were omitted completely from the model. A graphical representation of the ellipsoid-plate model is shown in Figure 8, along with a line drawing of the actual FB-111A for reference.

b. **Improvements to the Baseline Model**. Verification of the baseline model against measured data at a single frequency allowed the systematic addition of components to improve the model's performance over the range of elevation angles. A detailed discussion of the aircraft model's evolution is contained in Chapter IV (Results). The final model configuration and the actual FB-111A are shown in Figure 9.

(a) Actual Side View   (b) Model Side View

(c) Actual Front View   (d) Model Front View

(e) Actual Top View   (f) Model Top View
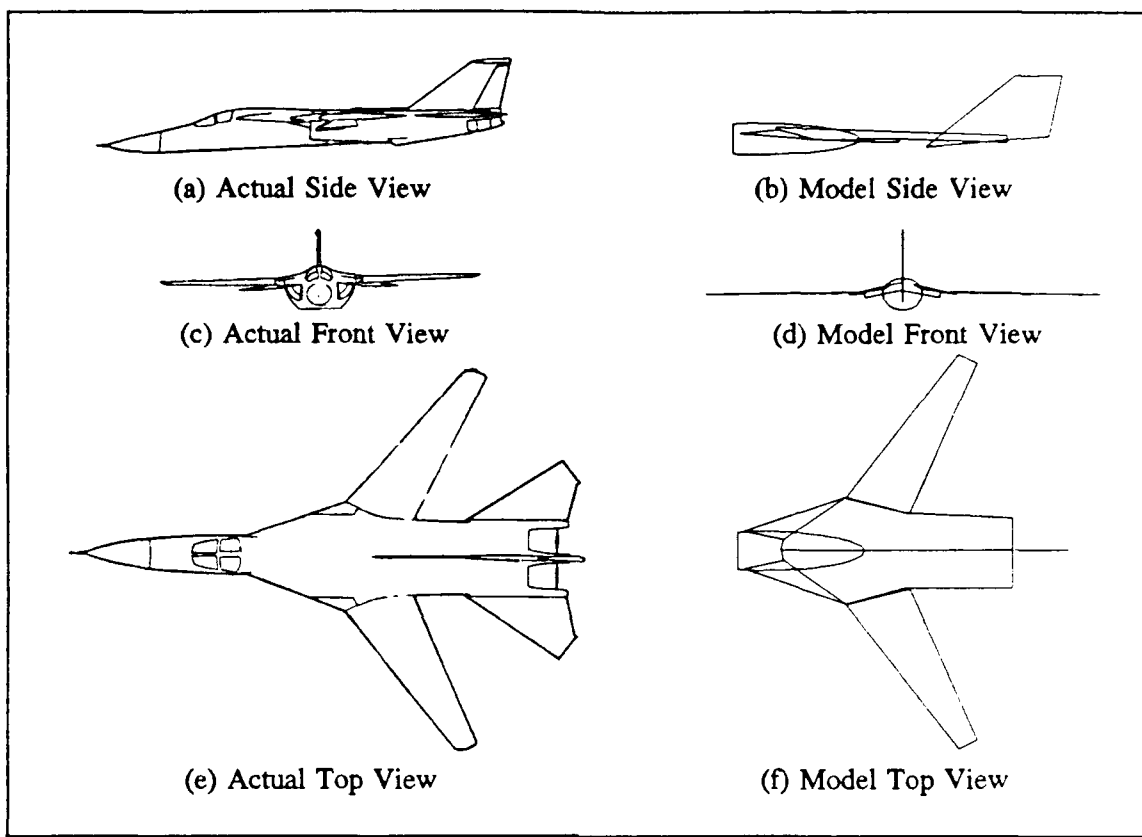
Figure 8.   FB-111A: Actual and Baseline Geometric Model

c.   <u>Empirically Determining Plate Model Parameters from Measured</u>

<u>Antenna Pattern Characteristics</u>.   It was possible to deduce the parame-

ters of a plate model that could cause given characteristics in the

measured antenna radiation patterns.   While this technique does not

provide a "unique solution" to the causes of antenna pattern phenomena,

the ability to estimate additional model features to improve its

performance against a given set of measured data is useful (if a

complimentary demonstration of the model is desired).   More importantly,

deduction of model characteristics from the measured data provides

insight into possible physical causes of radiation pattern phenomena.

(a) Actual Side View   (b) Model Side View

(c) Actual Front View   (d) Model Front View

(e) Actual Top View   (f) Model Top View
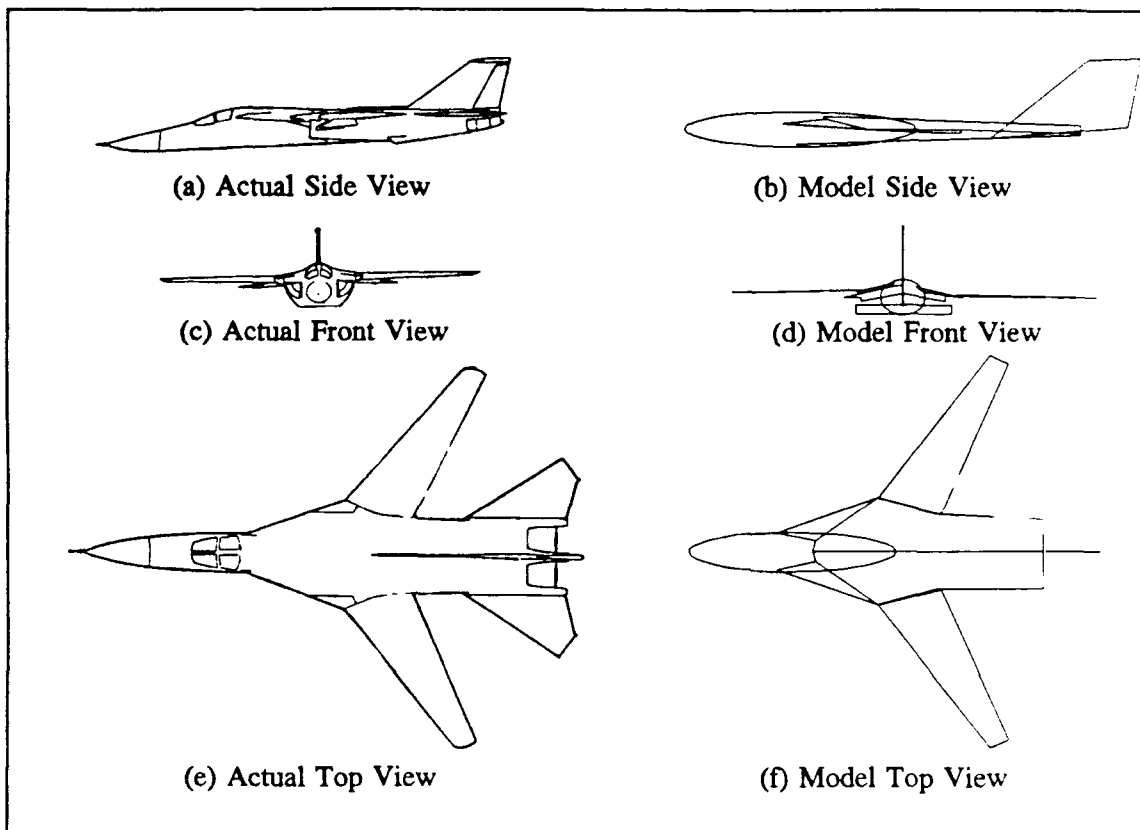
Figure 9.   FB-111A: Actual and Final Geometric Model

Figure 10 shows a radiation pattern that has the characteristics of the basic spiral antenna (peaking at about 315° azimuth) and FB-111A structure (reduced gain in the region of the cockpit windscreen and the effects of fuselage curvature). Besides these basic features, there is a noticeable pattern of three peaks and two nulls in the region from 30° to 75° azimuth. The locations of these peaks and nulls and basic knowledge of the FB-111A fuselage surface characteristics allow deduction of a mechanism that could cause these pattern features. Figure 11 shows the geometry for finding the approximate dimensions of a model plate that would cause the same basic pattern characteristics observed in the measured data. An observer in the far field on a ray directed

32
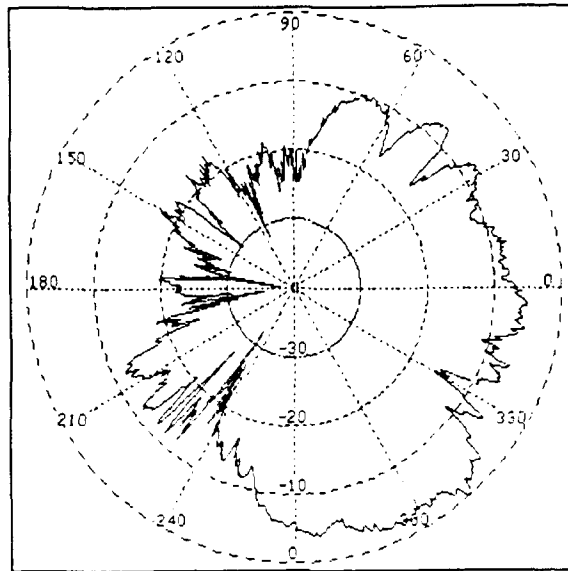
Figure 10. FB-111A Spiral Antenna
Radiation Pattern at 6.5
GHz, +10° Elevation
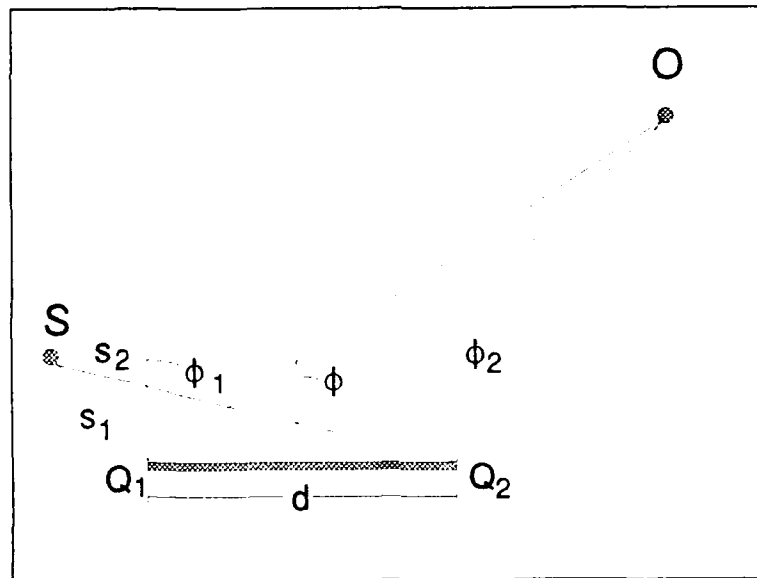
Figure 11. Geometry for Determining Model Plate
Parameters

from the center of the plate along azimuth angle ϕ will sense, among

other field components, diffracted fields from edges Q_1 and Q_2. The

diffracted field components from Q_1 and Q_2 will add constructively or

destructively depending on their relative phases at the observation point. Since the distances (s_1 and s_2) from the source (S) to the points of diffraction are fixed, variations in the relative phases of the diffracted fields from Q_1 and Q_2 at the point of observation are due to changes in the position of the observer. In the far field, the position of the observer can be defined by the angle ϕ (from the center of the plate) which also approximates the angles ϕ_1 and ϕ_2. The phase difference ($\Delta\psi$) between the diffracted fields at Q_1 and Q_2 is found through Eq (4).

$$\Delta\psi = \beta_0 d \sin(\phi) \qquad (4)$$

If the orientation of the plate edges can be reliably estimated (as in the case of fuselage access plates), the approximate effective distance between edges Q_1 and Q_2 in terms of the illumination wavelength (λ) can be found from the angular locations (ϕ_{m1} and ϕ_{m2}) of adjacent peaks in the diffraction pattern from Q_1 and Q_2 using Eq (5).

$$\pm 2\pi \approx \beta_0 d \sin(\phi_{m1}) - \beta_0 d \sin(\phi_{m2}) \rightarrow$$
$$d \approx \frac{\pm\lambda}{\sin(\phi_{m1}) - \sin(\phi_{m2})} \qquad (5)$$

where the sign is chosen so that d is a positive number. Results of using this equation are shown in Chapter IV.

5. __Antenna Model__. This study required modeling the radiation characteristics of 2 inch spiral antennas (General Dynamics part number 16VE

233-1, serial number 104) used for the actual measurements (Rome Air Development Center 1984b:1-2). The Airborne Antenna Radiation Pattern Code allows modeling antennas as monopoles or arbitrarily oriented aperture slots on the surface of the aircraft fuselage. For scattering from aircraft whose geometry is uniform in the z dimension, various line source models are also available in the code. The model of the cavity-backed spiral was developed using an array of monopole antennas to simulate the typical free-space pattern of the spiral. The monopole antenna was used because its far-field azimuth plane pattern for vertical polarization is identical to an isotropic source. A planar array of monopole antennas was developed so the array's far-field pattern closely resembled that of a spiral antenna boresighted at 315° in the pattern plot coordinate system shown in Figure 5. To minimize complexity and provide an array that could easily be input into the UTD model, an array of nine antennas (a three by three array) was selected for pattern synthesis. This paragraph describes development of the array parameters.

a. **Beam Synthesis**. Before the monopole antenna's maximum could be steered to the 315° azimuth, it required shaping into one major lobe of sufficient beamwidth and small backlobe to simulate the cavity-backed spiral antenna's radiation pattern. A convenient way of shaping the response of an omnidirectional antenna (such as a monopole) is to combine more than one antenna into a linear array. The radiation pattern for a linear array can be predicted from the location and pattern factor of each antenna and the magnitude and phase of its current excitation. For the far-field azimuth pattern of a monopole,

the pattern factor is unity. Referring to Figure 12, the far-field
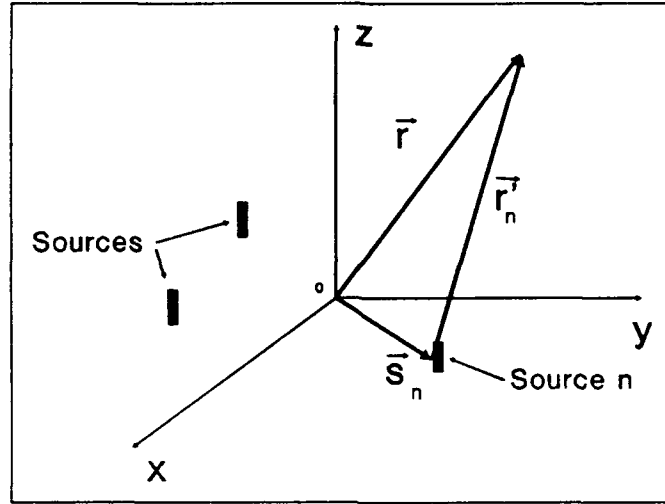
Figure 12. Geometry for an Arbitrarily-
Spaced and -Excited Linear
Array

normalized total field ($\vec{E}_T$) in the x-y plane for the combination of z-
directed infinitesimal elements is given by Eq (6) (Balanis, 1982:107).

$$\vec{E}_T = \sum_{n=1}^{M} \vec{E}_n$$

$$\vec{E}_n = I_n e^{-j\alpha_n}\, \hat{\theta}\frac{e^{-j(\beta_o r_n')}}{r_n'}$$

(6)

where
$\vec{r}_n'$ = vector from source n to the observer

r_n' = $|\vec{r}_n'|$

r_n' ≈ r (for magnitude computation in the denominator)

r_n' ≈ r − $\vec{s}_n \cdot \vec{r}$ (for phase computation in the exponential)

$\vec{r}$ = vector from the origin to the observer

$\vec{s}_n$ = vector from the origin to the source n

β_0 = free-space wave number

α_n = phase angle of excitation current in source n

I_n = magnitude of excitation current in source n

M = number of array elements

A binomial distribution of excitation current magnitudes was selected to achieve a small backlobe. The array factor for a uniformly-spaced array of elements excited with current magnitudes with a binomial distribution from one end to the other and spaced half-wavelength or closer has minimum backlobes (Balanis, 1982:241). For the three-element x-axis array in Figure 13 of uniformly-spaced, binomially excited elements
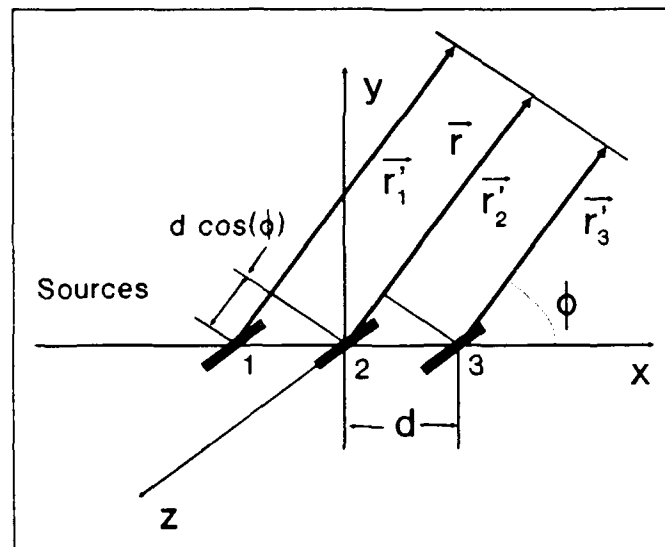
Figure 13. Geometry for Planar Array on
the x-y Plane

whose inter-element phase difference is a constant (α), the array factor can be simplified. Since, for three elements, the binomial coefficients are 1, 2, 1, Eq (6) simplifies to Eq (7).

$$\vec{E}_T = 2\,\vec{E}_0\,(1e^{-j\alpha}\,e^{-j\beta_0 d\cos(\phi)} + 2e^{j0} + 1e^{j\alpha}\,e^{j\beta_0 d\cos(\phi)})$$

$$= 2\hat{2}\,\vec{E}_0\,[1 + \frac{1}{2}\,(e^{j[\alpha + \beta_0 d\cos(\phi)]} + e^{-(j[\alpha + \beta_0 d\cos\phi])})\,] \qquad (7)$$

$$= 2\hat{2}\,\vec{E}_0\,[1 + \cos(\alpha + \beta_0 d\cos(\phi))]$$

By absorbing all the constant coefficients into a normalized amplitude and using the trigonometric identity for power relations of cosine functions, Eq (8) for the magnitude of the normalized array factor ($|E_T|$) resulted.

$$|\vec{E}_T| = \cos^2(\frac{\alpha + \beta_0 d\cos(\phi)}{2}) \qquad (8)$$

From Eq (8) it can be seen that peaks occur where the argument of the cosine function is an integer multiple of π as in Eq (9).

$$\frac{[\alpha + \beta_0 d\cos(\phi)]}{2} = n\pi \;\rightarrow$$

$$\alpha + \beta_0 d\cos(\phi) = 2n\pi \;\rightarrow \qquad (9)$$

$$\beta_0 d\cos(\phi) = 2n\pi - \alpha$$

$$n \in \{0, 1, \ldots\}$$

Selecting 1/4 wavelength spacing and steering the maximum of the array factor to occur $\phi = 0°$, the relative phase difference between adjacent elements in the of the array in Figure 13 was found to be $-90°$. By defining the current in the element at the origin to have magnitude of 1 and phase of $0°$, the normalized array factor in Figure 14, matching beamwidth and backlobe criteria for simulation of the cavity-backed spiral antenna, was achieved.
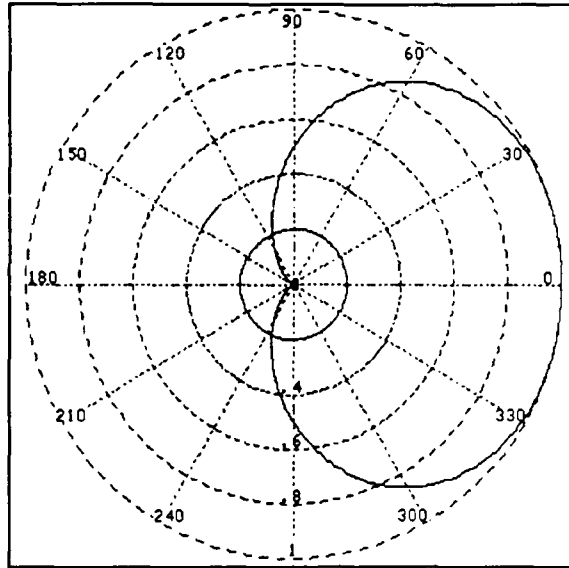
Figure 14. Array Factor in the x-
Axis Direction

b. **Beam Steering**. To steer the beam shaped above to the appropri-
ate azimuth angle (ϕ) for the antenna in this study (315°), a second
array factor was developed. Forming a second binomially-excited,
uniformly-spaced, three-element array along the y-axis, the relative
phases of element excitation currents for 1/4 wavelength inter-element
spacing was found using Eq (9). The parameters for the y-axis array
were used to construct an array of the x-axis arrays found above. The
normalized field pattern for the resultant planar array is plotted in
Figure 15. Inter-element spacing was then adjusted empirically to 0.24
wavelengths and inter-element phase relations were made to be -86.4°
(along x) and -78.4° (along y) so that the shape of the steered beam
closely approximated that of a cavity-backed spiral. Figure 16 shows
the planar array model pattern compared to the measured radiation
pattern of a 2 inch cavity-backed spiral antenna mounted in a free-space

39
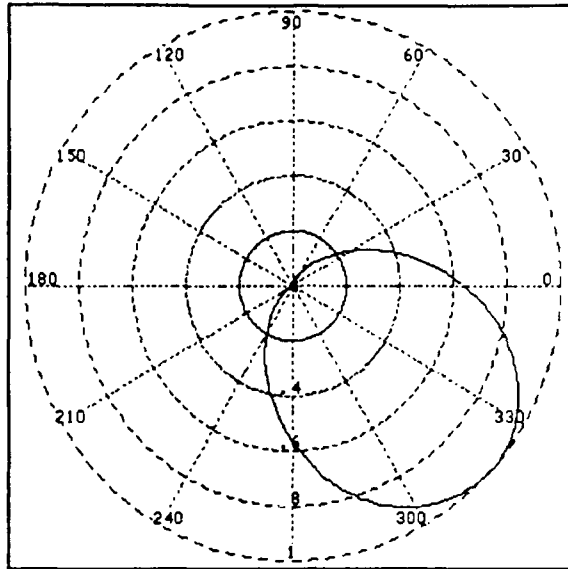
Figure 15. Normalized Field Pattern
for a Binomial Array
Steered to 315°

location (tip of the FB-111A horizontal stabilizer) (Rome Air Develop-
ment Center, 1984b:Appendix B). The measured plot values were rotated
to coincide in angle with the antenna under study. There is close
agreement between the model and measured data. The array parameters are
summarized in Table I. The monopole locations input to the scattering
model must be specified in physical dimensions (such as inches), so the
locations listed in Table I in wavelengths were converted to inches for
each frequency studied. A computer program was written in FORTRAN-77
specifically to perform the conversion. The output of the model for the
antenna mounted on a very large fuselage ellipsoid with no other struc-
ture present is shown in Figure 17. The model output shows the influ-
ence of the curved fuselage on the spiral antenna pattern for azimuths
around the nose.

40

Table I. Array Element Excitation Parameters

Element	z position (wavelengths)	y position (wavelengths)	Magnitude (Dimension-less)	Phase (Degrees)
1	-0.24	0.24	.25	-8.0
2	0.0	0.24	.50	78.4
3	0.24	0.24	.25	164.8
4	-0.24	0.0	.50	-86.4
5	0.0	0.0	1.00	0.0
6	0.24	0.0	.50	86.4
7	-0.24	-0.24	.25	-164.8
8	0.0	-0.24	.50	-78.4
9	0.24	-0.24	.25	8.0

6. **Software and Processing**. This paragraph describes the software used in this study and provides an overview of manual and computer processing necessary to execute the antenna radiation pattern model.

a. **Software Used**.

1) **Airborne Antenna Radiation Pattern Code**. The FORTRAN-77 program NEWAIR3.FOR was first modified to eliminate calls to plotting routines that were not resident on the host computer used for this study. A sample of the program's input and printed output files is included in Appendix A. Complete descriptions of the input and output

41

Normalized Field Pattern   Normalized Gain Pattern
  (Dimensionless)   (dB$_i$)
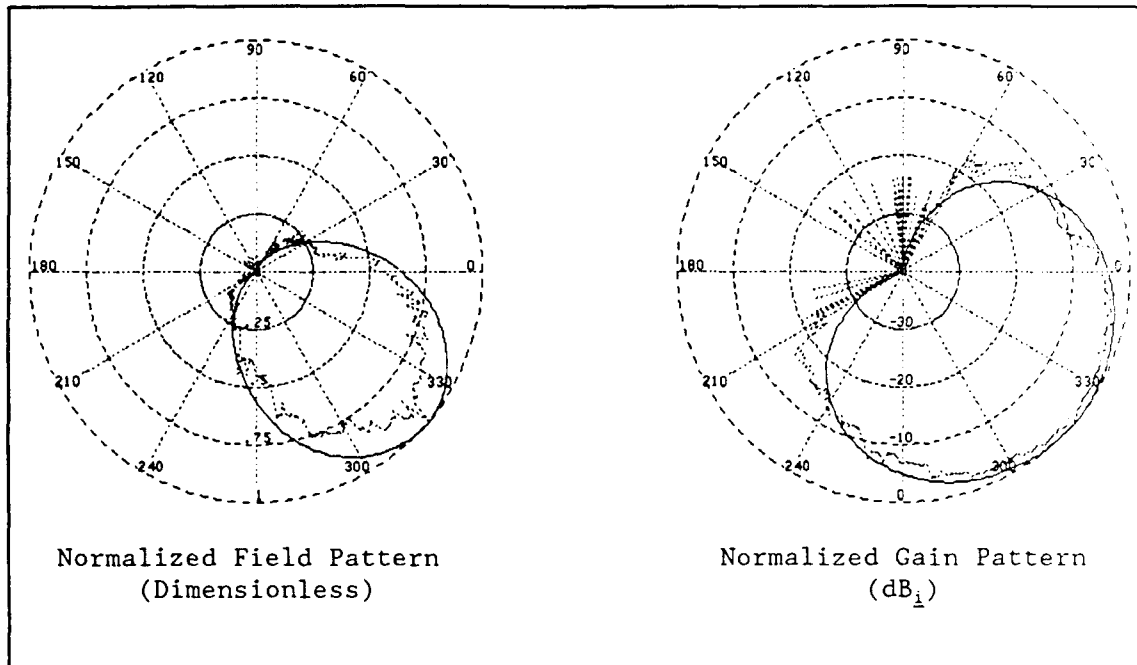
Figure 16. Modeled (Solid Line) and Measured (Dotted Line) Field (a)
and Gain (b) Patterns for a 2 inch Cavity—Backed Spiral
Antenna

data are found in the *Airborne Antenna Radiation Pattern Code User's
Manual* (Burnside and others, 1985:20—67).

      2) **Data Format Utility**. A FORTRAN—77 program was written to
interpret the NEWAIR3 binary output files (FORnnn.DAT) into ASCII files
of angle/power data pairs. The program ran either interactively or from
a VMS procedure (.COM) file and wrote output files of normalized (to
unity as the highest absolute power level) data for vertical and
horizontal polarization in both absolute values and referenced decibel
values. Decibel values were written so that the lowest value was zero
and the highest value was a user—defined value. This data convention
for decibels facilitated constructing polar plots of the output.
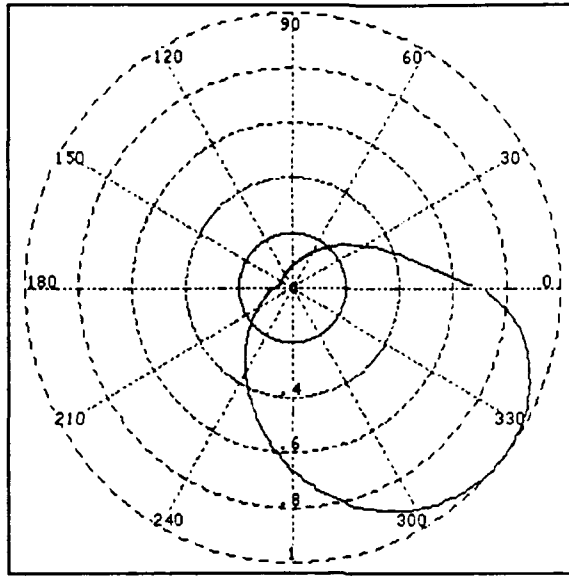
Figure 17. Output of the UTD Model
for Spiral Antenna on a
Very Large Ellipsoid

3) **Planar Array Pattern Factor Calculation Program**. This

program calculates the array pattern factor for a planar array. Array

parameters are entered interactively at program prompts by the user.

The program assumes an array on the x-y plane, and outputs the normal-

ized (to unity) pattern factor for a specified conic cut. The conic cut

can be specified as a plot in polar ϕ for a fixed value of polar θ or as

a plot in θ for a fixed value of ϕ. The output ASCII file (PLANAR.DAT)

consists of ordered pair of angle (radian) and field (dimensionless)

values.

4) **Program to Convert Planar Array Parameters to NEWAIR3 Input**

File Format. This program converted planar array parameters from

PLANAR.FOR into the units used by the Airborne Antenna Radiation Pattern

Code. The spatial dimensions convenient for empirically determining the

43

required array parameters (position in wavelength) were converted by AM.FOR to the source position coordinate system (radius [in inches, feet, or meters] and angle [in degrees] of the vector fixing the array element on the surface of the fuselage) used in the code.

5) **Program to Decollate Measured Antenna Pattern Data**. This program read standard Rome Air Development Center Antenna Pattern Magnetic Tape Format data (Rome Air Development Center, 1982:1-6) into separate files for each antenna, frequency, polarization, and elevation angle for individual plotting.

6) **Plotting Software**. Plots for this report were generated using a personal computer and the public-domain program LABGRAPH.EXE. A screen-capture utility was used to interface the plots to the report text word processor.

b. **Manual Processing**.

1) **Entering Aircraft Model Dimensions**. Manual processes included converting the dimensions of the aircraft into fuselage and plate parameters for input to the model. A ruler graded in hundredths of an inch and hundredth scale drawings were used to obtain aircraft dimensions. To facilitate computation of model parameters, a scientific spreadsheet (MathCAD®) was used to generate plots of ellipse curvature and to fix the locations of model plate corners so the plates would be flat.

2) **Handling Datafiles**. The Airborne Antenna Radiation Pattern Code and format utility were run in a batch process (either may be run

interactively), necessitating the generation of data files. VMS

procedure files were used to automate some of the file handling opera-

tions, but manual intervention was necessary to review and plot data.

IV Results

1. **Introduction**. This chapter contains the study results, discussing the measured data used as the basis for evaluating the model output and the specific findings for the nine frequencies and five elevation angles examined.

2. **Discussion of Measured Antenna Patterns**. The data used to verify the output of the radiation pattern model in this study came from a test of a proposed but rejected configuration for RWR antenna installation. The test antennas were installed as shown in Figure 18. In this config- uration, there was little isolation of the antenna housings from the aircraft fuselage, and no special preparation of the fuselage surface is evident in the photograph from which Figure 18 was made. The measured patterns had a consistent lobing structure of peaks and nulls over the azimuths $0° < \phi < 180°$. There are no characteristics of the antenna or basic aircraft shape that account for these pattern features, which may be the result of interaction between the two antennas themselves or diffraction from gaps in the fuselage surface forming the antenna ground plane. The fuselage surface near the antenna consists of a number of access plates, and the bonding between adjacent plates may be imperfect resulting in a discontinuity in the surface near the antenna, for which moment-method modeling would be appropriate. The hypothesis that the observed lobing is due to fuselage surface cracks is substantiated through comparison of patterns for vertical and horizontal polarizations shown in Figure 19. This figure that shows the pronounced lobing exists
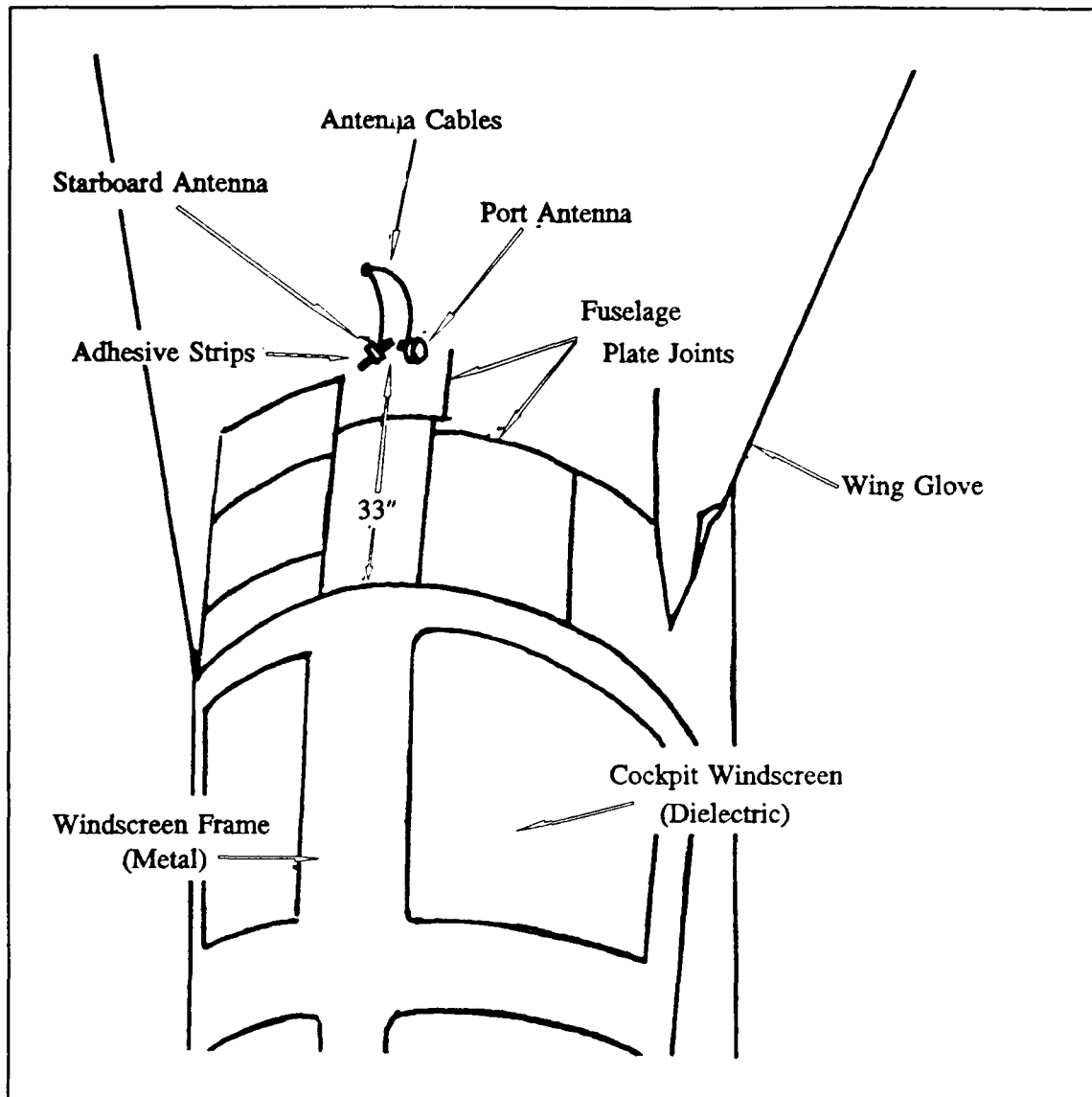
Figure 18. Test Installation of Spiral Antennas on FB-111 (from Rome Air Development Center, 1984b:5)

only for vertical polarization. For vertical polarization, horizontal cracks in the fuselage represent discontinuities in the surface currents supported by electric field component in the plane of incidence. Whatever its cause, the lobing is consistent between the starboard antenna (used for comparison in this study) and its mirror image on the

47

(a) +10° Elevation   (b) +20° Elevation
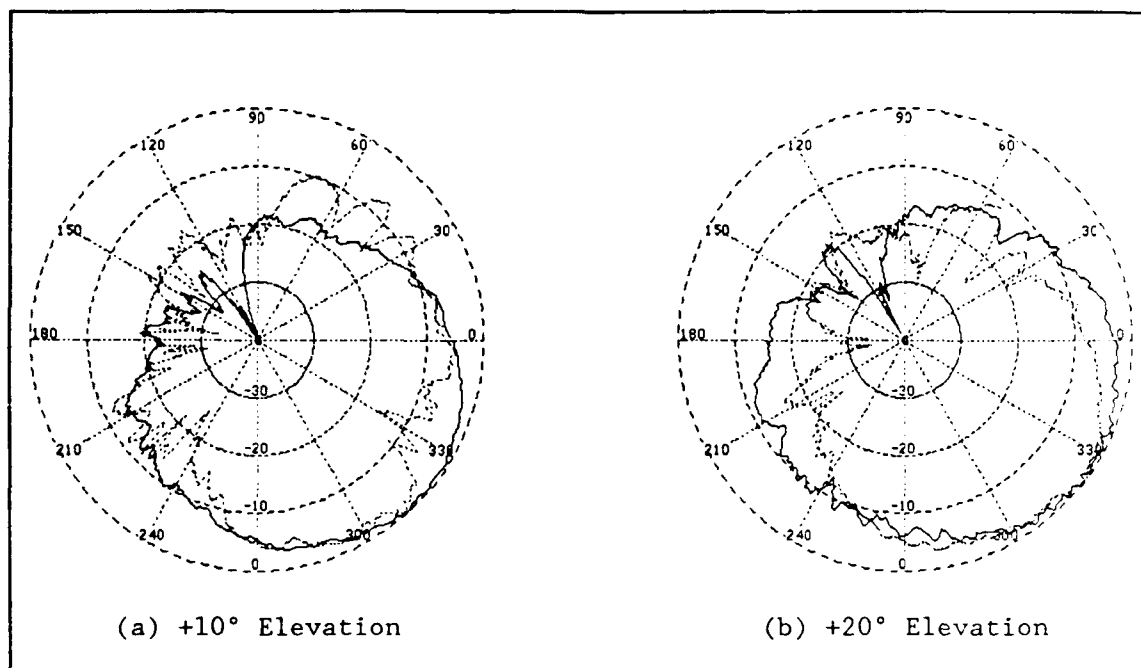
Figure 19. Measured FB-111A Spiral Antenna Pattern at 6.5 GHz: Horizontal (Solid Line) and Vertical (Dotted Line) Polarization

port side. The data for the two antennas is plotted in Figure 20 and Figure 21. The high degree of symmetry between the port and starboard antenna patterns is also observed at all other measured frequencies. The aircraft model was modified several times to isolate the cause of the lobing structure by adding small plates to duplicate the measured pattern using UTD. As discussed in paragraph 7 (below), success could be achieved for a given elevation angle, but no single model configuration could be found that gave acceptable results at all elevation angles of interest. If the lobing is due to the effects of discontinuities in the aircraft fuselage, scale model measurements would also fail to predict the phenomenon without painstaking detail in the model and antenna mounting. The differences between the modeled data below and the actual data represent the reality of modeling antenna systems: not
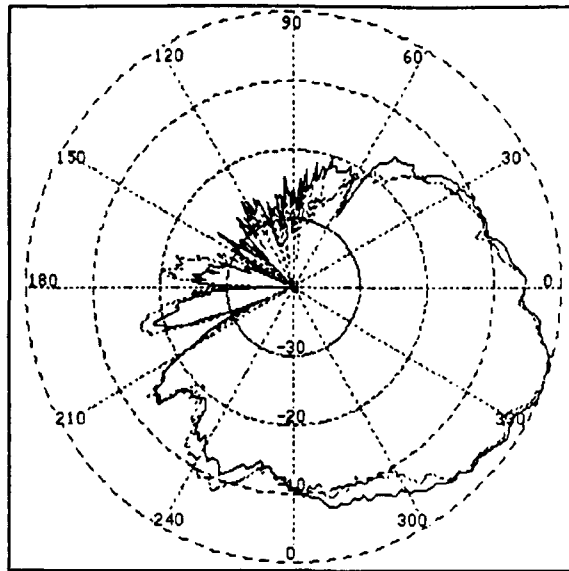
Figure 20. Measured Starboard (Sol-
id Line) and Mirror-
Image of Port (Dotted
Line) Antenna Patterns,
6.5 GHz, 0° Elevation

all characteristics of the measured results can be predicted through a

single modeling technique (mathematical or otherwise).

3. **Refinement of the FB-111A Geometric Model**. To explore the accuracy

of the FB-111A baseline model, 6.5 GHz was chosen as the model verifica-

tion frequency. 6.5 GHz was chosen because it was very near the

midrange of the frequencies for which measured data was available. The

baseline model was used to generate antenna pattern predictions for

+20°, +10°, 0°, -10°, and -20° elevation angles. The predicted patterns

were compared to corresponding measurements. The pattern plots were

used to identify inaccuracies in the baseline FB-111A model. The FB-

(a) −20° Elevation   (b) −10° Elevation

(c) +10° Elevation   (d) +20° Elevation
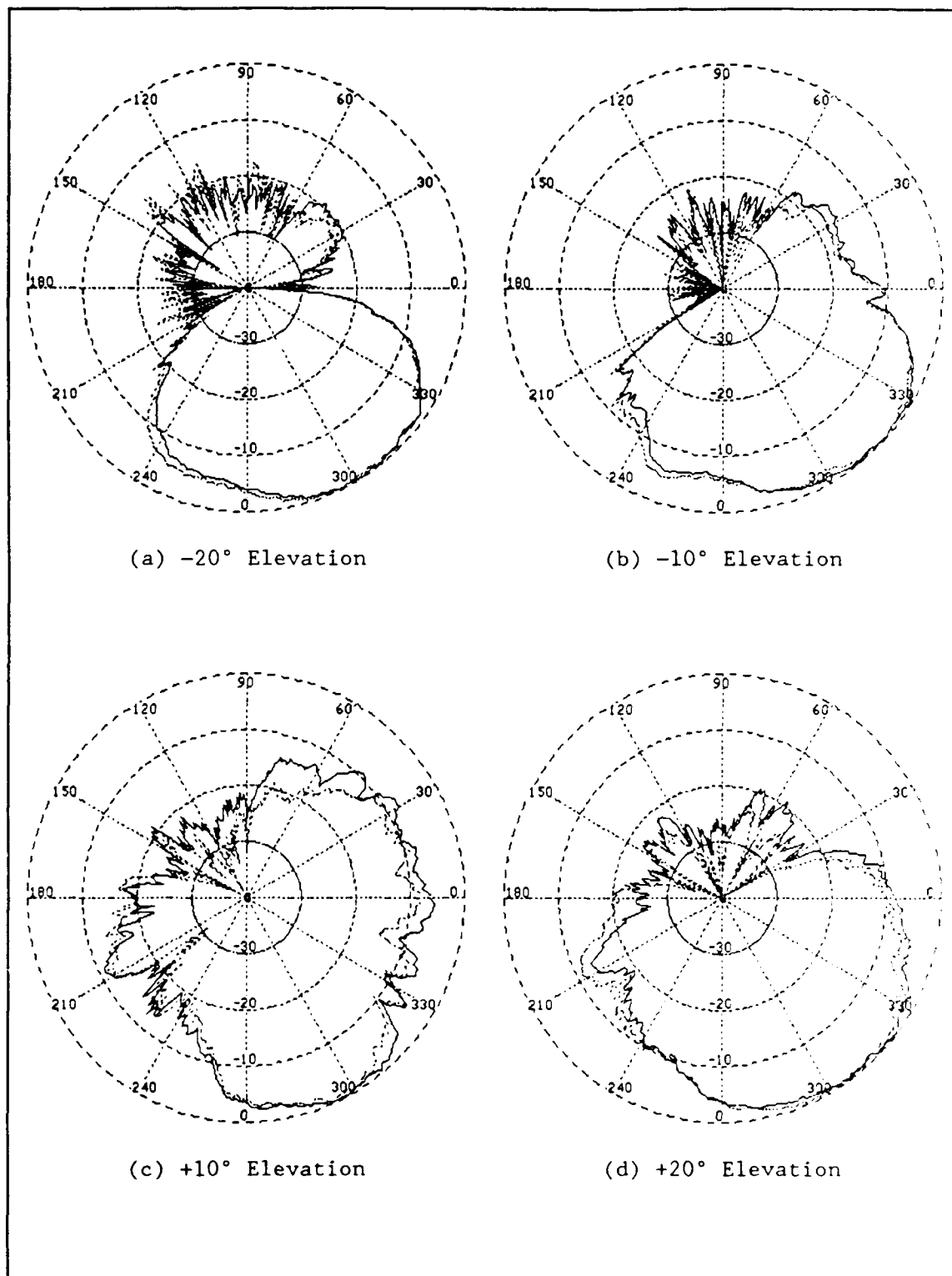
Figure 21. FB−111A Measured Spiral Antenna Pattern at 6.5 GHz: Starboard (Solid Line) and Mirror Image of Port (Dotted Line)

50

111A model was then refined iteratively to minimize the total error over
the five elevation angles measured. The optimized FB-111A model was
then used as the basis for studying the overall model's performance at
various frequencies. This paragraph describes the evolution of the
final FB-111A model.

a. **Results With Baseline Model**.

1) **Principal Plane Pattern**. The baseline model was successful
in outlining the overall shape of the measured pattern. At 0° elevation
as shown in Figure 22, the measured data exhibited more of a peak in
gain than the model output, and also showed significantly more pro-
nounced lobing (peaks and nulls) on the port side of the aircraft
(0° < ϕ < 180°) than the model predicted. The absence of pattern lobes
on the port side of the aircraft is also a noticeable feature at other
elevation angles.

2) **Patterns at Other Elevation Angles**. Figure 23 contains
patterns for elevations other than the principal azimuth plane.

a) **Pattern at -20° Elevation**. At -20° elevation, the most
notable additional difference between the model prediction and the
measured data is directly at the nose (ϕ - 0°). The model fails to
predict the extremely small response of the system here. Noticeable in
this plot are the discontinuities at ϕ - 30° and ϕ = 335°. These spikes
in the pattern are due to the plot passing through two caustic regions
The Airborne Antenna Radiation Pattern Code computed the caustic surfac-
es to occur at -17° and -22° elevation for the model execution from
which this plot was taken. With so short an angular spike extent, this
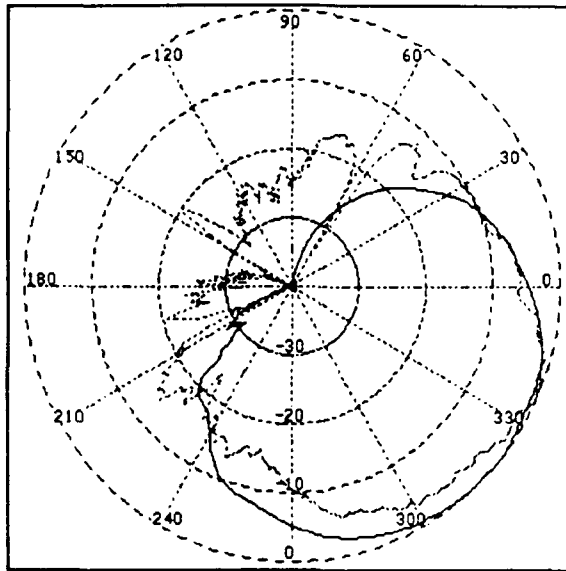
Figure 22. Principal Plane Pattern
Using Baseline FB-111A
Model at 6.5 GHz Pre-
dicted (Solid Line) and
Measured (Dotted Line)

plot illustrates how a continuous solution could be obtained by interpo-

lating the UTD solution through the caustic region. However, in this

study, the fuselage model was eventually modified to eliminate the chop

simulating the cockpit. With this modification to the model, the caus-

tic regions were shifted beyond the elevation angles of interest.

3) **Pattern at -10° Elevation**. Here the predicted pattern has

its best correlation with the measured data. Except for the lack of

lobing already noted above for the port side of the aircraft and a small

caustic region at ϕ - 348°, the model succeeds in predicting the shape

of the measured radiation pattern.

(a) −20° Elevation (b) −10° Elevation

(c) +10° Elevation (d) +20° Elevation
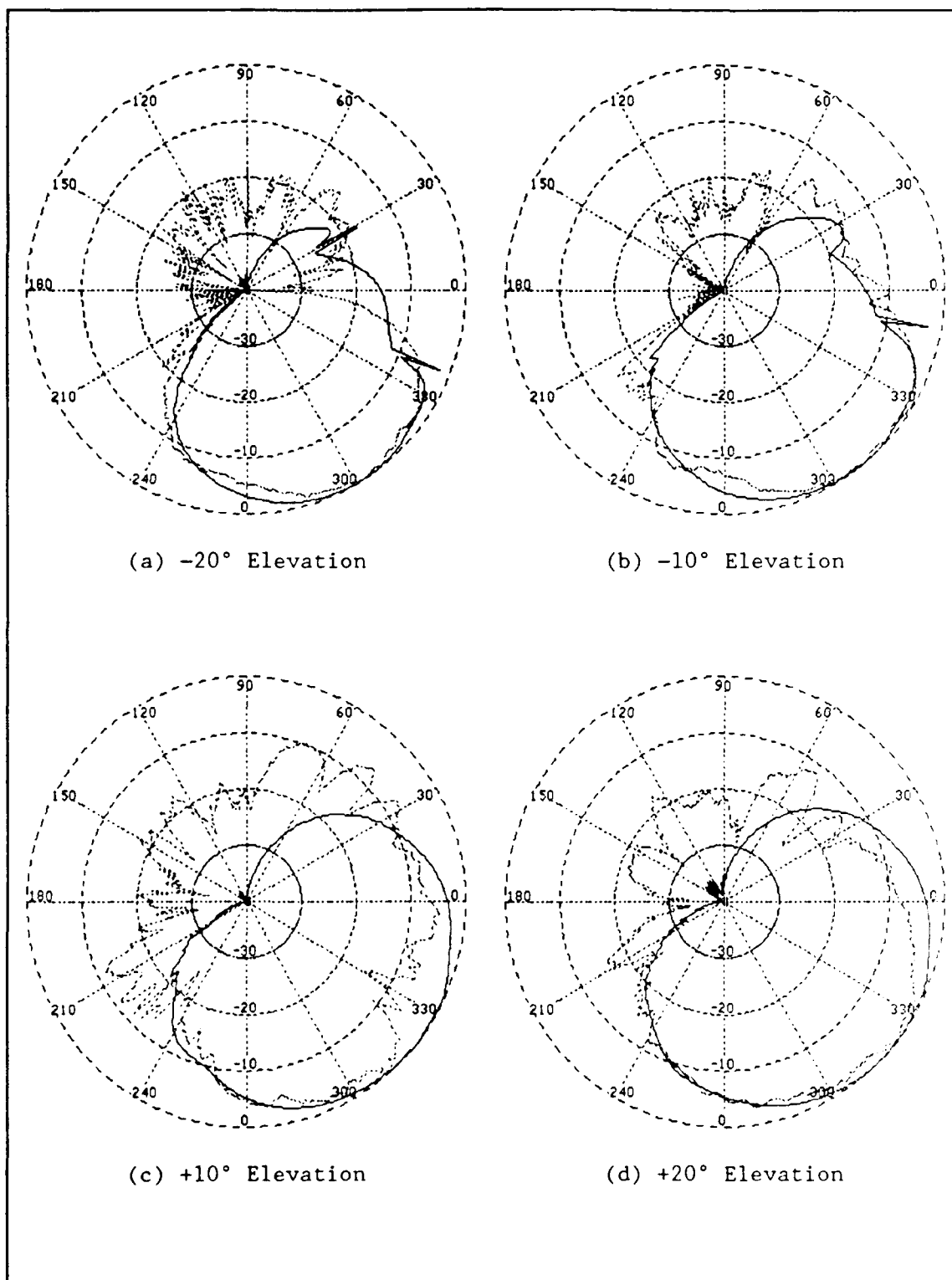
Figure 23. FB–111A Antenna Pattern at 6.5 GHz: Measured (Dotted Line) and Predicted (Solid Line) Using Baseline Model

a) **Pattern at +10° Elevation**. In this pattern, there appear to be a significant number of features in the measured data not predicted by the model. A different normalization of the predicted pattern could have resulted in closer correlation in absolute value with the measured data. Certain features, such as the very low measured response at 330° and 235° and the significant lobing for the angular region 0° < ϕ < 180°, are missing from the model output.

b) **Pattern at +20° Elevation**. At this elevation angle, the model successfully predicts the region where the pattern peaks, but misses all the lobing evident in the measured data.

b. **Model Refinement**. The results with the baseline model and several trial models of the nose section forward of the rear cockpit bulkhead indicated that a continuous curvature at the aircraft nose would result in the closest correlation with measurements. The intent of the Airborne Antenna Radiation Pattern Code is reflected in the final model configuration: it represents the aircraft as accurately as possible in its basic form using model elements larger than one wavelength.

4. **Effects of Varying Frequency on Model Accuracy**. Once the baseline model was refined, the scattering model was run for all measurement frequencies to investigate the effect of varying frequency on model accuracy.

a. **Frequency 1: 2.5 GHz**. Figure 24 and Figure 25 show the radiation patterns at 2.5 GHz for the various elevation angles. Some of the remarkable gain at the backlobe of the system may be due to diffractions from the fuselage surface and windscreen interface. There may

54

Figure 24. FB-111A and Spiral Antenna Model at 2.5 GHz, 0° Elevation Predicted (Solid Line) and Measured (Dotted Line)

also be interaction between the antenna housing (a conductor) and the fuselage surface. This complex relationship between the fuselage surface and the antenna could not be modeled using only the basic shape of the aircraft. The patterns contain useful information on the antenna system's general performance near the antenna boresight. The effects of the starboard wing glove (abrupt change in gain where the wing glove shadows the antenna from the observer) occur in the model results for $-10°$ elevation at about $4°$ azimuth ahead of the same effects in the measured data. This angular separation between the model predictions and the measured results (explored later in this report) remains consistent at all measured frequencies. The magnitude of the diffraction effects in the wing glove region ($210° < \phi < 240°$) is higher than

(a) −20° Elevation

(b) −10° Elevation

(c) +10° Elevation

(d) +20° Elevation
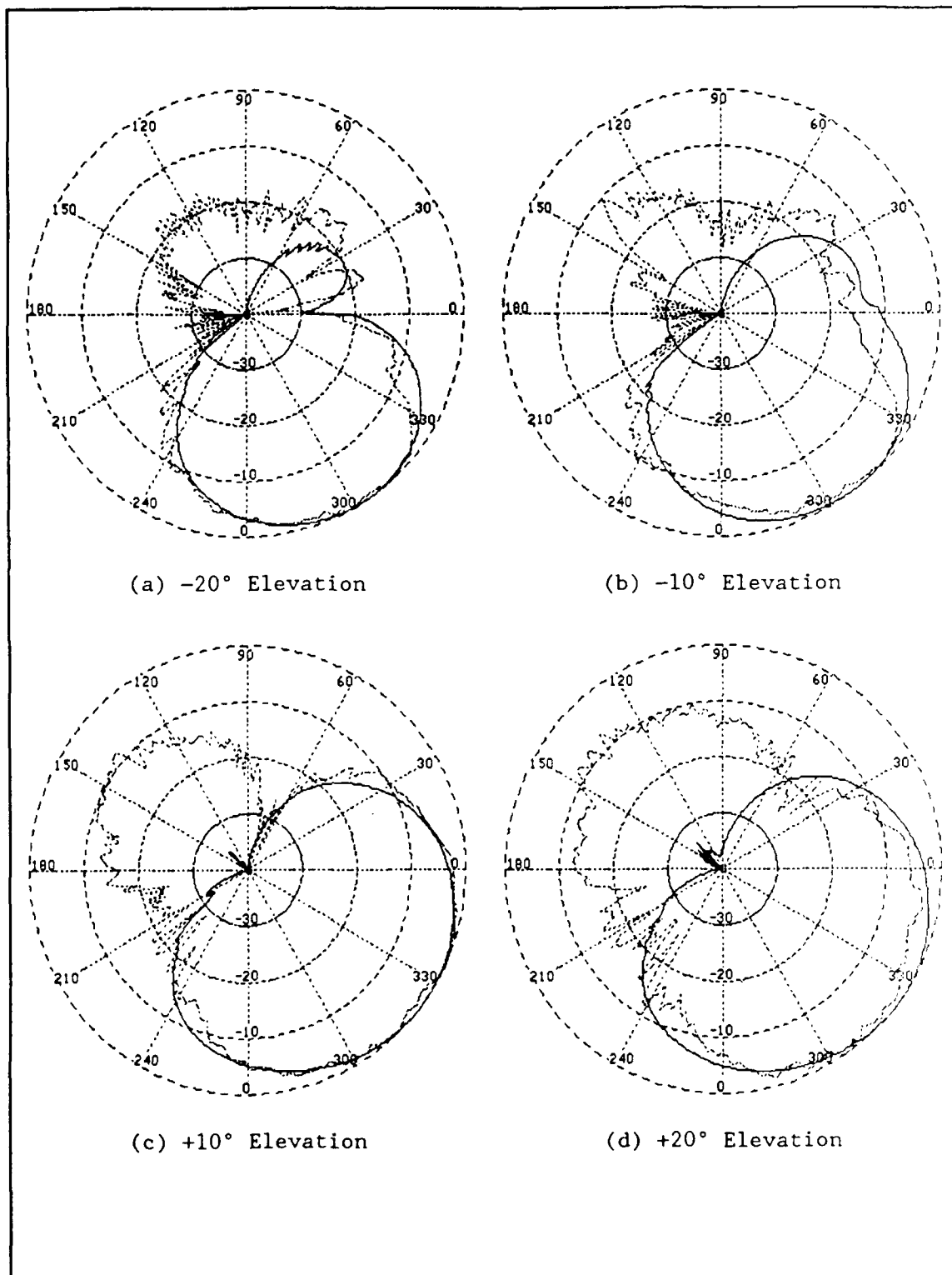
Figure 25. FB−111A Antenna Pattern at 2.5 GHz: Measured (Dotted Line) and Predicted (Solid Line)

predicted. The transition from the outboard edge of the wing root to the wing was relatively smooth in the model. On the actual aircraft, there may be a discontinuity at the junction of the wing root and wing or fuselage that diffracts more than the model predicted. The general nature of the diffraction effects (an angular region of jaggedness in the pattern) occurs as predicted by the model. The effects of the fuselage curvature are apparent in the −10° and −20° elevation plots over the region 40° in azimuth either side of nose-on. The difference between measured and predicted gain in the region around the nose in the −10° elevation plot (about 4 to 6 dB) could be attributable to the finite conductivity of the cockpit windscreen. The very low gain due to complete shadowing of the source by the fuselage exactly at nose-on azimuth at −20° elevation is clearly predicted by the model.

b. **Frequency 2: 5.0 GHz**. Plots for this frequency are shown in Figure 26 and Figure 27. At 0° elevation, the model predicts from 6 to 8 dB higher gain than measured for azimuth angles from 270° to 300°. There are also differences between measured and predicted gain at +10° elevation from 270° to 330° azimuth. The model consistently overesti- mates the gain in these regions. The mechanism for the measured reduction in gain, which recurs at other frequencies, is not apparent in the basic structure of the aircraft. Perhaps the most striking differ- ence from predicted gain and reality is seen in the plot for +20° elevation near the nose. The measured 15 dB reduction in gain, which would be highly significant to the antenna system performance, was consistent in the port antenna pattern. The phenomenon may be due to the fuselage surface or the windscreen interface diffractions, which
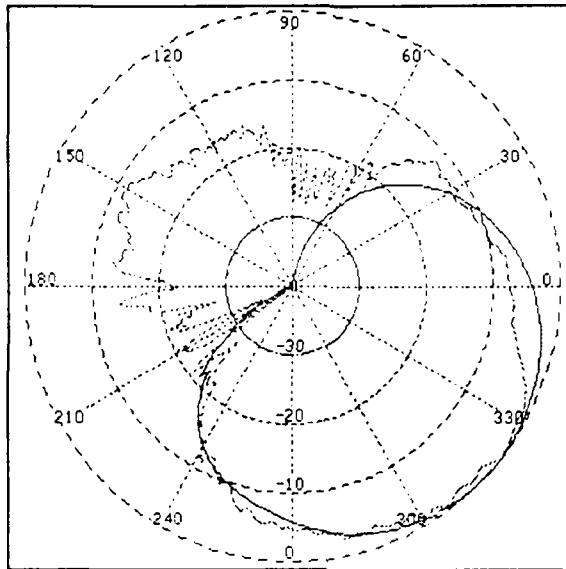
Figure 26. FB-111A and Spiral An-
tenna Model at 5.0 GHz,
0° Elevation Predicted
(Solid Line) and Mea-
sured (Dotted Line)

could not be modeled using UTD alone.

c. **Frequency 3   6.5 GHz.** Figure 28 and Figure 29 show the results
with the "optimized" model at the same frequency at which it was
developed from the baseline. There is close agreement between predicted
and measured data at 0°, -10°, and -20° elevations. Above the aircraft,
the pronounced effects of the fuselage discontinuities are present in
the measured data and absent from the predictions. The predicted pat-
tern for +10° elevation has two major differences from the measured
data. The measured lobing from 45° to 70° azimuth is absent from the
prediction, as is the null in the observed pattern at 330° azimuth.
Either or both these observed phenomena could be due to discontinuities
in the fuselage surface.

(a) −20° Elevation   (b) −10° Elevation

(c) +10° Elevation   (d) +20° Elevation

Figure 27. FB-111A Antenna Pattern at 5.0 GHz: Measured (Dotted Line) and Predicted (Solid Line)

Figure 28. FB-111A and Spiral An-
tenna Model at 6.5 GHz,
0° Elevation Predicted
(Solid Line) and Mea-
sured (Dotted Line)

d. **Frequency 4: 7.4 GHz**. Figure 30 and Figure 31 show the modeled

and measured patterns at this frequency. At 0° elevation, there is a 6

dB reduction in gain around 270° azimuth which the model did not

predict. At other elevation angles, there is close (4 dB) correlation

between the model results and the measurements, except for the reduced

gain apparent in the measured data at azimuths around the nose at +10°

elevation. There is also a null in the pattern for +10° elevation at

30° azimuth which the model did not predict. This null and the peaks in

the pattern at 40° and 55° azimuth could be due to diffraction from

cracks in the fuselage surface. No basic characteristic in the aircraft

geometry explains the presence of this these pattern features.

(a) −20° Elevation (b) −10° Elevation

(c) +10° Elevation (d) +20° Elevation

Figure 29. FB-111A Antenna Pattern at 6.5 GHz: Measured (Dotted Line) and Predicted (Solid Line)

Figure 30. FB-111A and Spiral An-
tenna Model at 7.4 GHz,
0° Elevation Predicted
(Solid Line) and Mea-
sured (Dotted Line)

e. **Frequency 5: 8.0 GHz**. Figure 32 and Figure 33 again show the
reduction in measured gain present at 270° azimuth at 0° elevation and
near the nose at +10° elevation. Similar to the results for lower
frequencies, the model did not predict the lobing characteristics in the
measured pattern from 30° to 75° azimuth, which is apparent at all 5
elevation angles at this frequency. Aside from these differences, the
predicted pattern shape generally agrees with the measured result and
would provide a useful estimate of the basic characteristics of the
antenna system's performance.

(a) −20° Elevation   (b) −10° Elevation

(c) +10° Elevation   (d) +20° Elevation

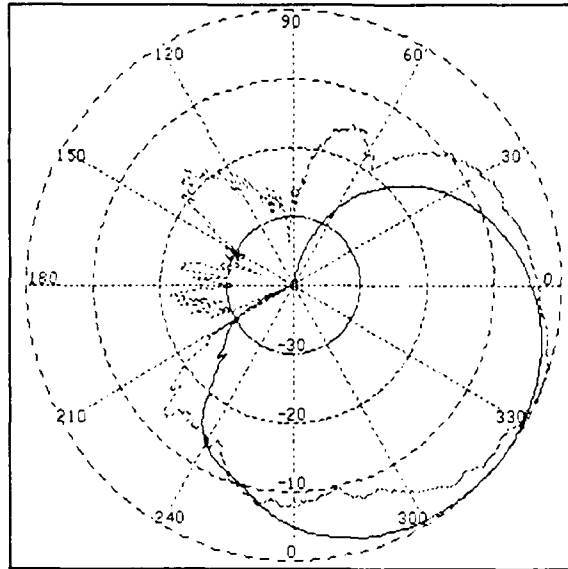Figure 31. FB-111A Antenna Pattern at 7.4 GHz: Measured (Dotted Line)
and Predicted (Solid Line)

Figure 32. FB-111A and Spiral Antenna Model at 8.0 GHz, 0° Elevation Predicted (Solid Line) and Measured (Dotted Line)

a. **Frequency 6: 9.3 GHz**. In Figure 34, there is a pronounced null in the measured pattern at about 265° azimuth, and a significant peak (of about -12 dB,) located at 210° azimuth, neither of which occur in the model result. The unexpected peak in the antenna's backlobe region could be s nificant because of its effect on angle-of-arrival estimates, which are often based on the relative power in the four antennas of an RWR system. Figure 35 shows the reduction in gain at azimuths around the nose at +10° elevation, consistent with measurements in the same region at other frequencies. The lobing seen from 0° to 180° azimuth is also consistent with patterns for other frequencies.

(a) −20° Elevation   (b) −10° Elevation

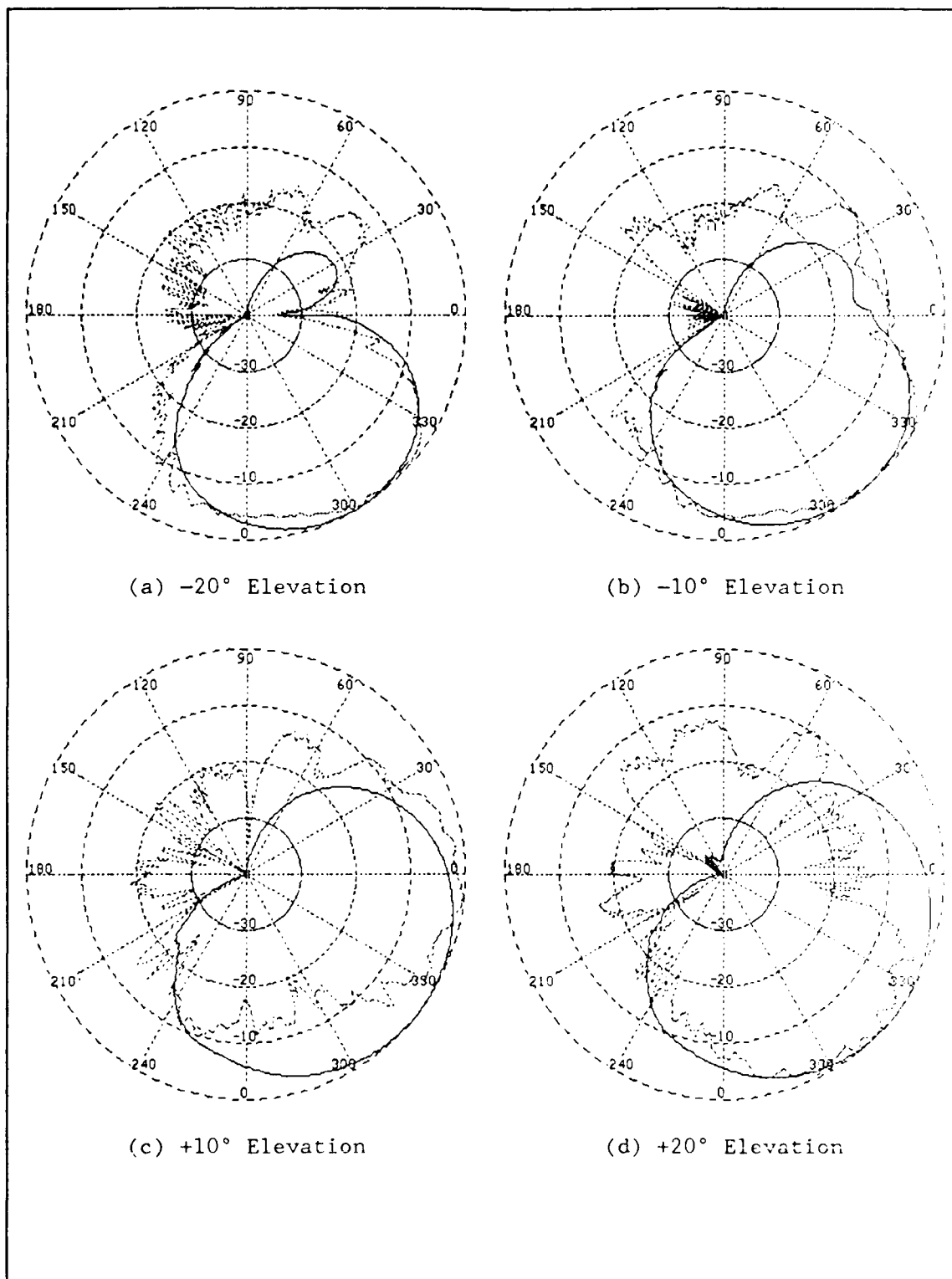(c) +10° Elevation   (d) +20° Elevation

Figure 33. FB-111A Antenna Pattern at 8.0 GHz: Measured (Dotted Line) and Predicted (Solid Line)
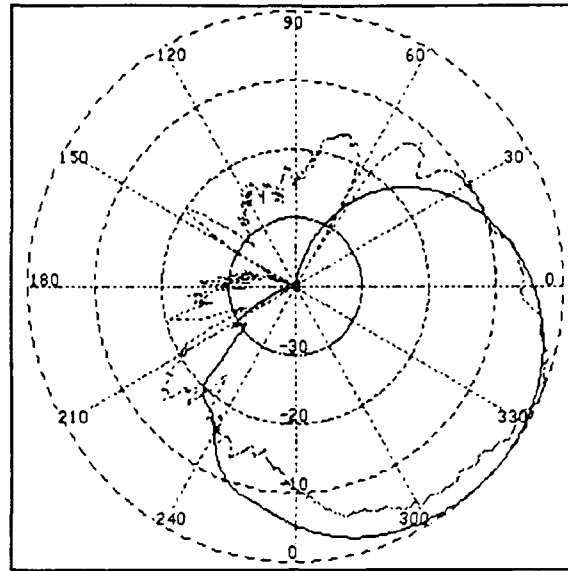
Figure 34. FB-111A and Spiral An-
tenna Model at 9.3 GHz,
0° Elevation Predicted
(Solid Line) and Mea-
sured (Dotted Line)

b. **Frequency 7: 10.0 GHz**. Figure 36 shows the reduced gain near

270° azimuth at 0° elevation, extending to 330° at this frequency. The

magnitude and extent of this angular region of reduced gain have major

significance to the system fed by this antenna system. The failure of

the model to predict this feature of the antenna pattern points to the

need for including additional effects (over and above UTD) in the model.

Figure 37 documents the gain reduction at 0° azimuth and pronounced

lobing from 0° to 90° azimuth at +10° elevation. The differences

between the predicted an measured patterns at this frequency are

consistent with the results at other frequencies.

(a) -20° Elevation   (b) -10° Elevation

(c) +10° Elevation   (d) +20° Elevation
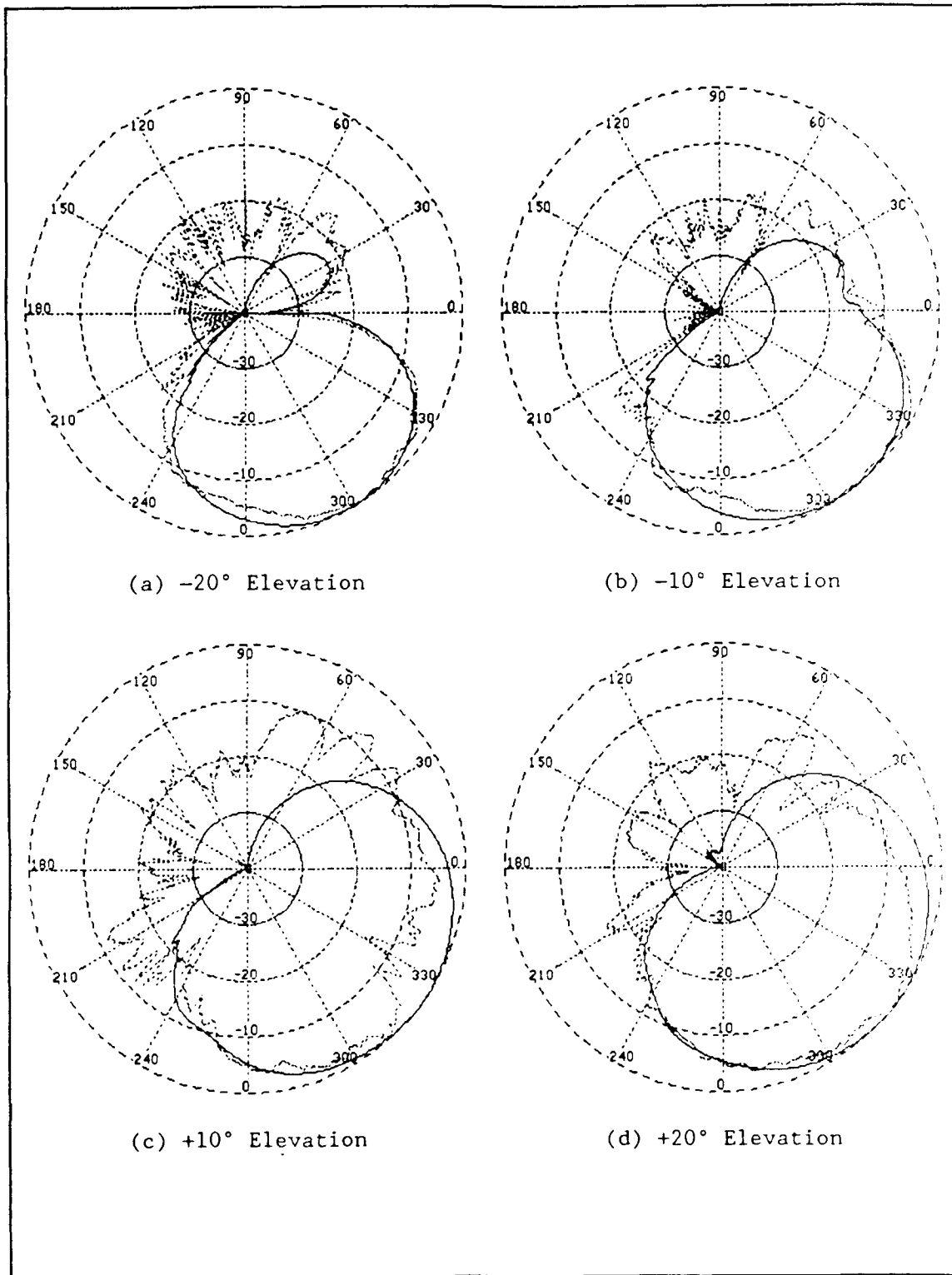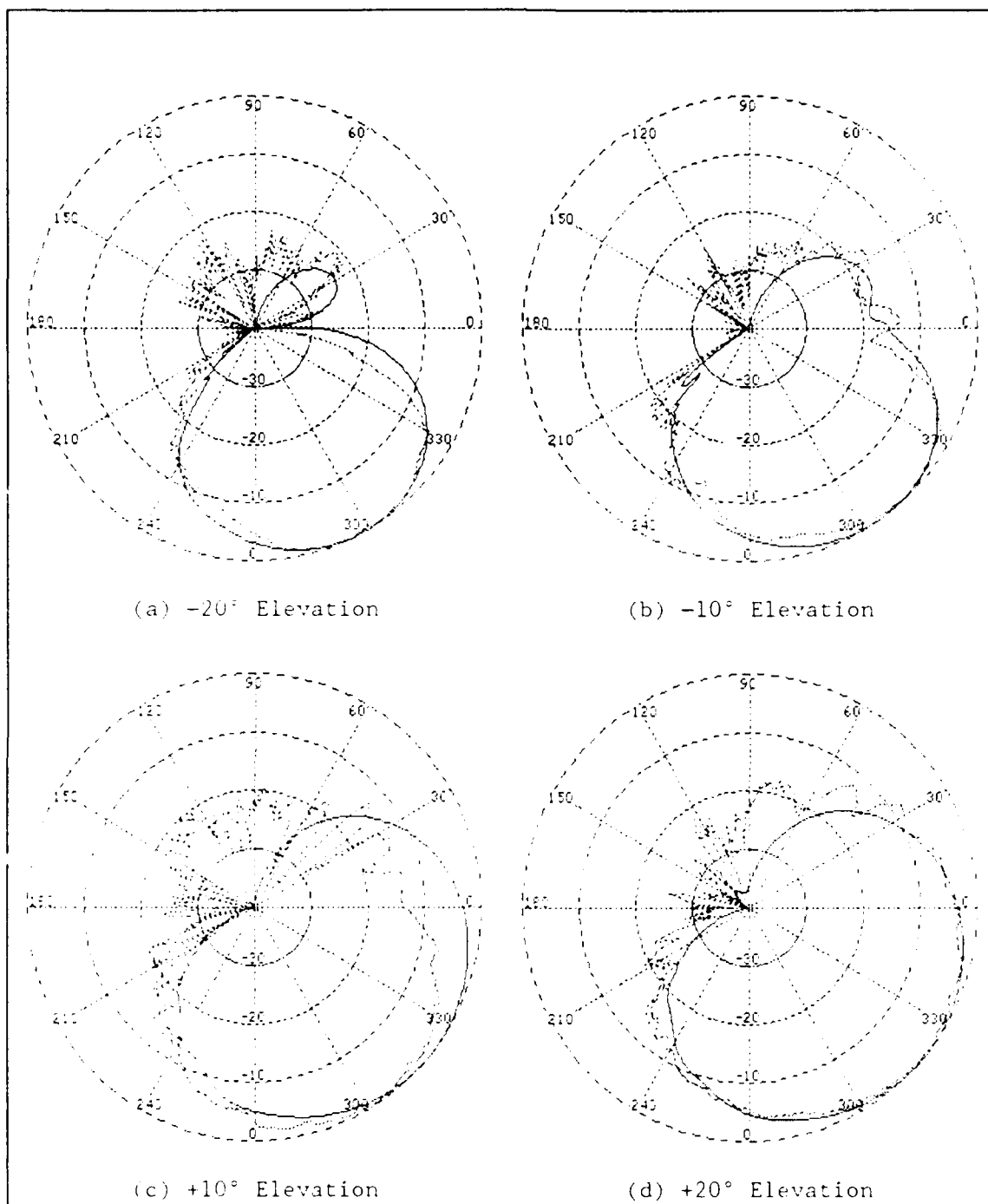
Figure 35. FB-111A Antenna Pattern at 9.3 GHz: Measured (Dotted Line) and Predicted (Solid Line)
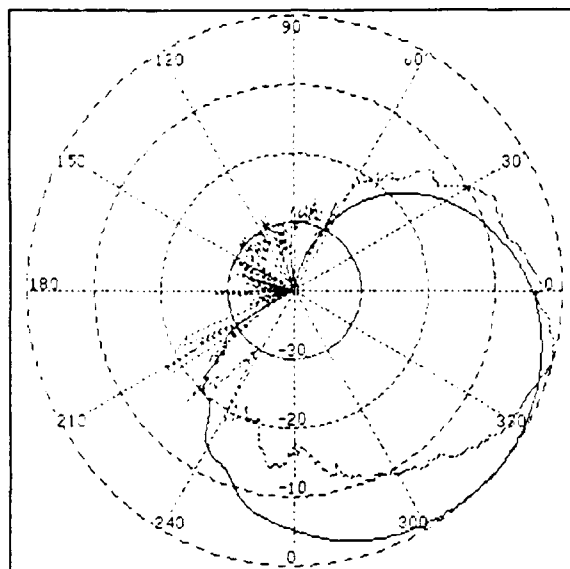
Figure 36. FB-111A and Spiral An-
tenna Model at 10.0 GHz,
0° Elevation Predicted
(Solid Line) and Mea-
sured (Dotted Line)

c. **Frequency 8: 12.9 GHz**. In Figure 38, the reduction in gain
seen at 270° in patterns for lower frequencies is shifted to 320°
azimuth. Figure 39 documents a smaller reduction (about 4 dB) in gain
at 0° azimuth at +10° elevation than is present at other frequencies.
There is also a noticeable (8 dB) reduction in gain at 320° azimuth at
+20° elevation. Consistent with antenna patterns for other frequencies,
the pronounced pattern of peaks and nulls from 0° to 180° is again
present in the measured data, especially for +10° elevation. These
features do not appear in the model results.

(a) −20° Elevation (b) −10° Elevation

(c) +10° Elevation (d) +20° Elevation
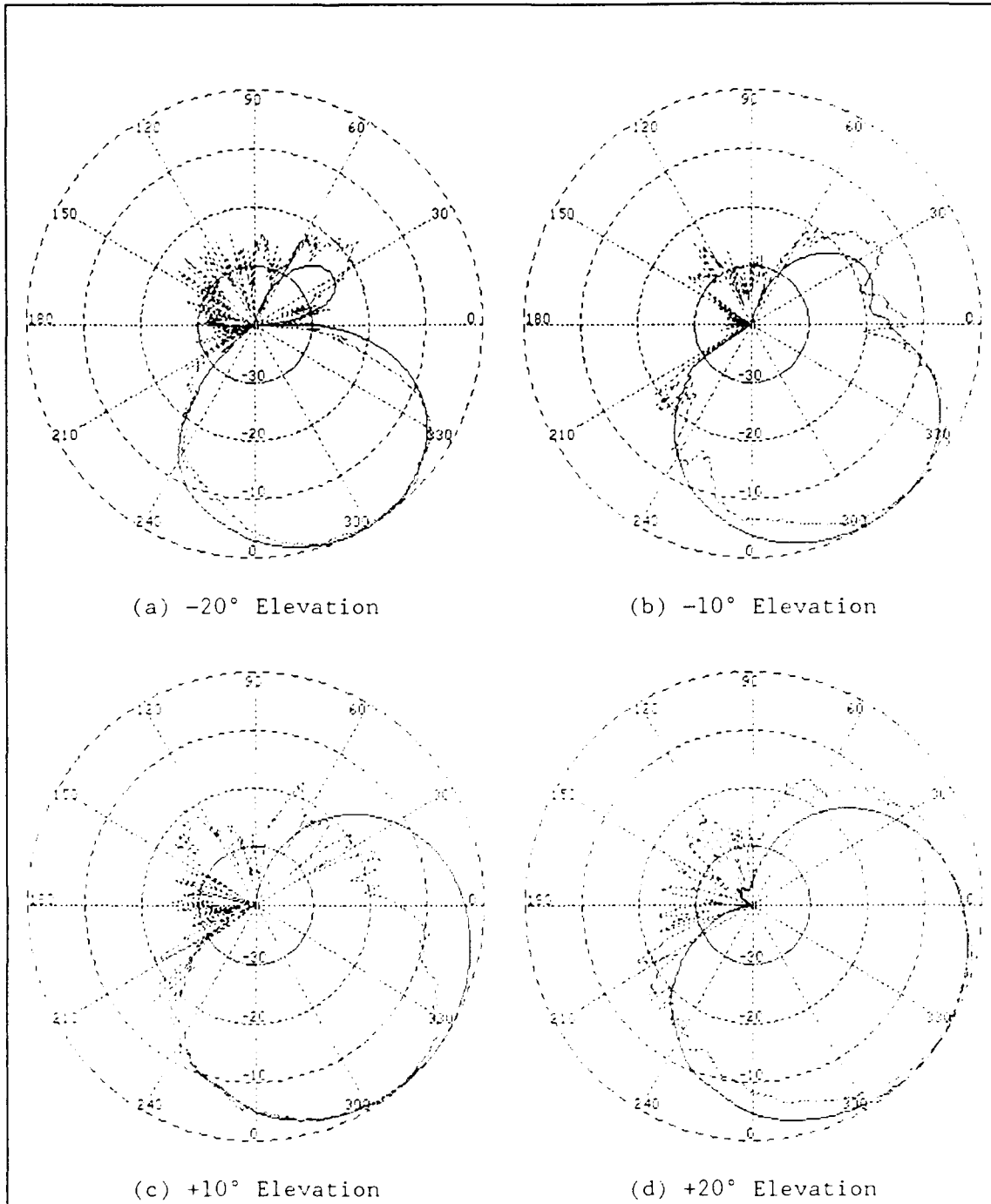
Figure 37. FB–111A Antenna Pattern at 10.0 GHz: Measured (Dotted Line) and Predicted (Solid Line)
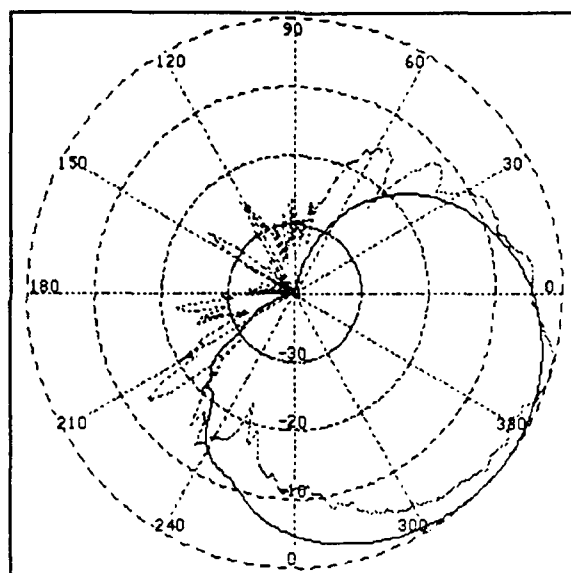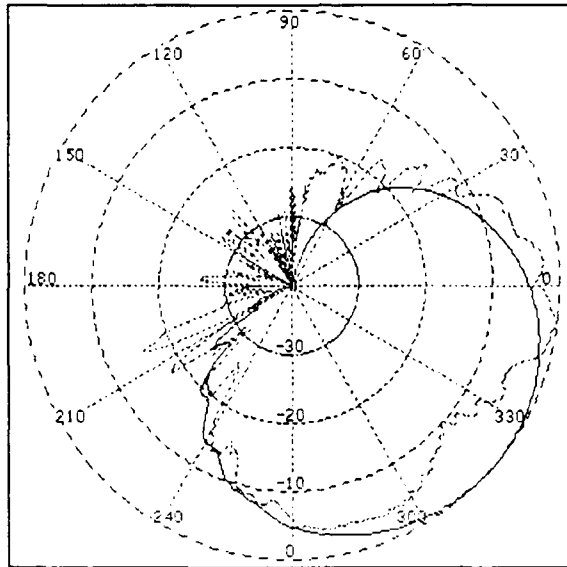
Figure 38. FB-111A and Spiral An-
tenna Model at 12.9 GHz,
0° Elevation Predicted
(Solid Line) and Mea-
sured (Dotted Line)

d. **Frequency 9: 15.0 GHz**. In Figure 40, the reduced gain seen at 270° azimuth at 10.0 GHz and lower is observed at about 330° azimuth. In Figure 41, the predicted pattern differs from the measured pattern by 7 dB at -10° elevation (near 4° azimuth). Interestingly, there is no reduction in gain evident at +10° elevation around the nose, but there is a drastic reduction in gain in this region at +20° elevation. Also at +20° elevation from 0° to 75° azimuth, there is a very periodic lobing structure present in the measured data that was not duplicated by the UTD prediction code using the aircraft model's basic shapes. Even at this, the highest frequency, model results clearly show that important scattering mechanisms in addition to the basic UTD shapes influence the performance of the antenna system.

(a) −20° Elevation   (b) −10° Elevation

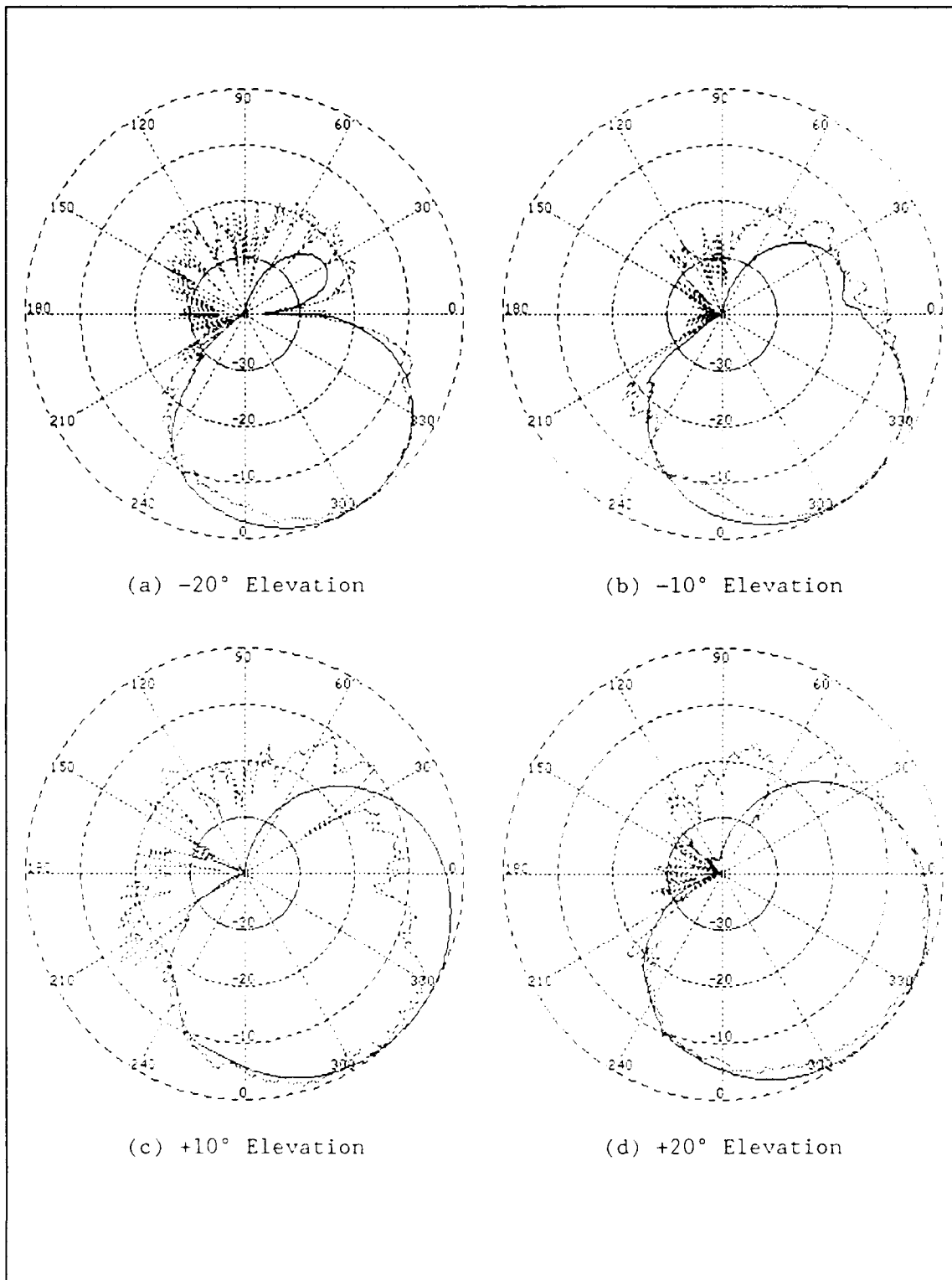(c) +10° Elevation   (d) +20° Elevation
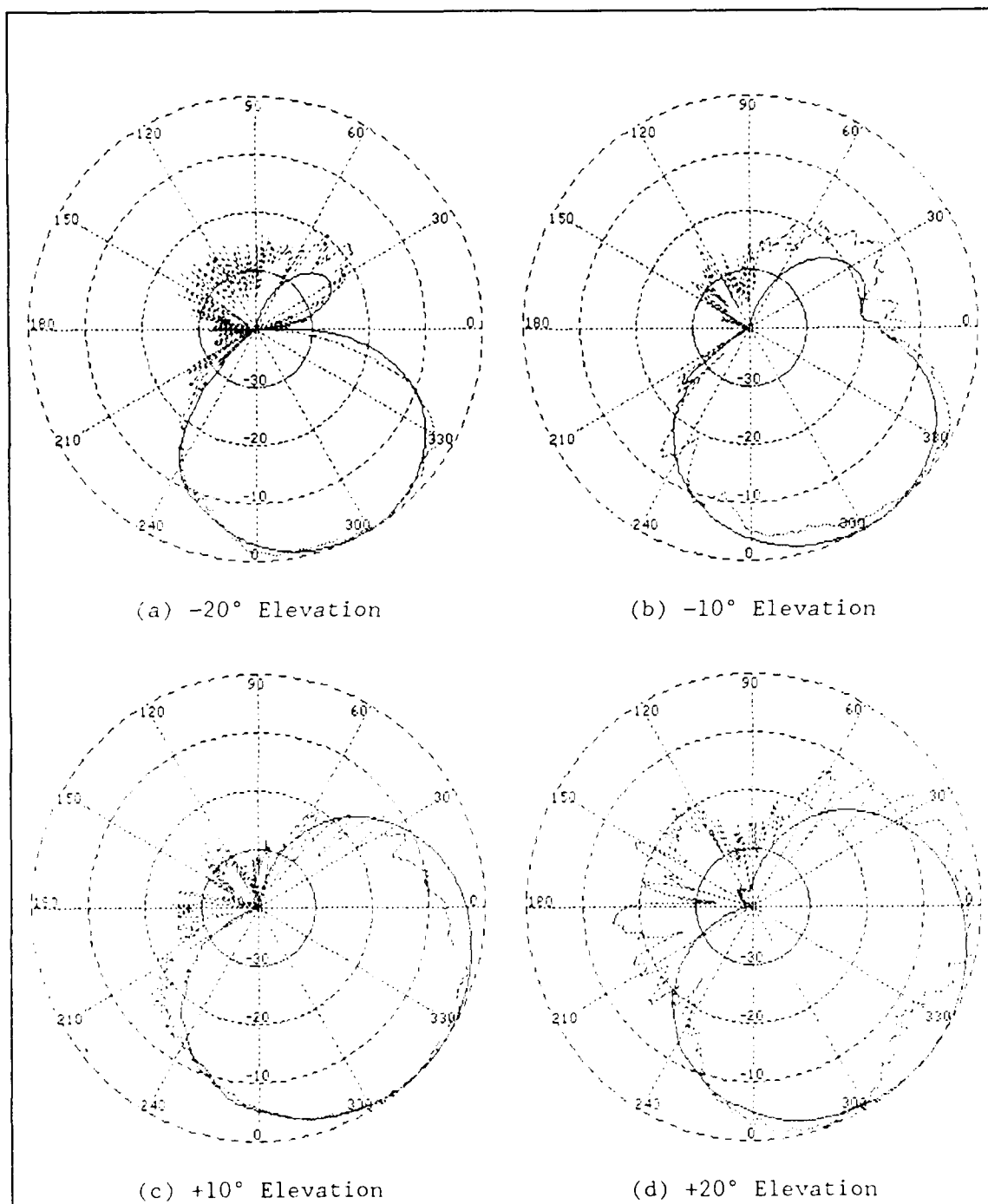
Figure 39. FB-111A Antenna Pattern at 12.9 GHz: Measured (Dotted Line) and Predicted (Solid Line)
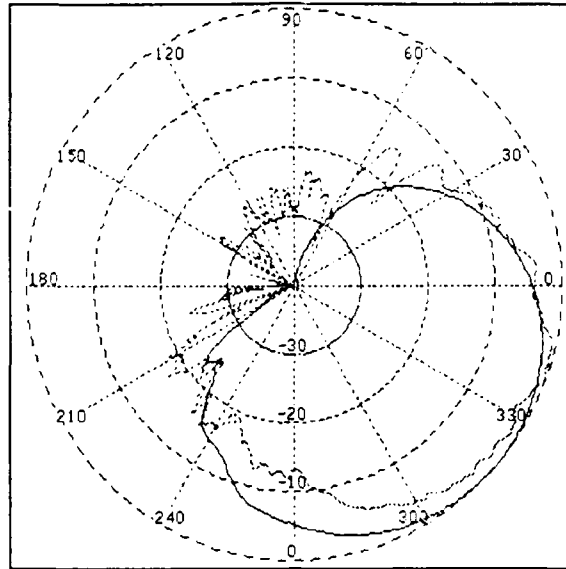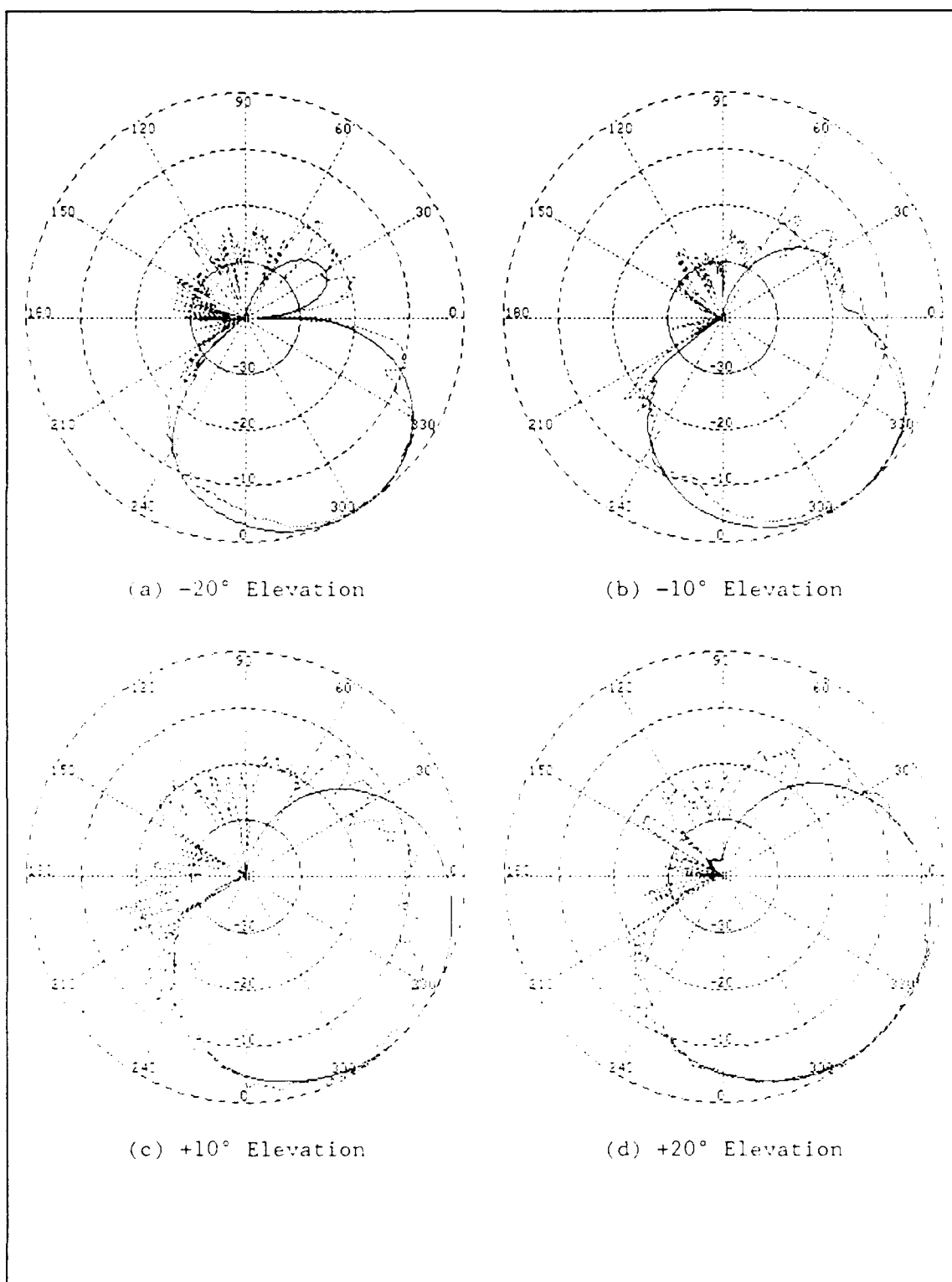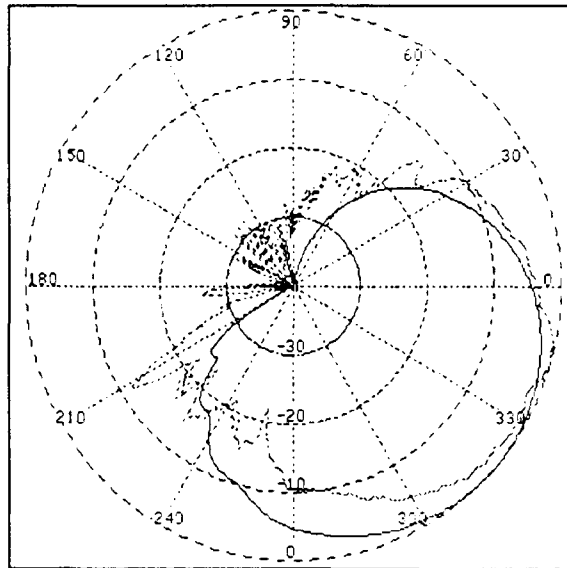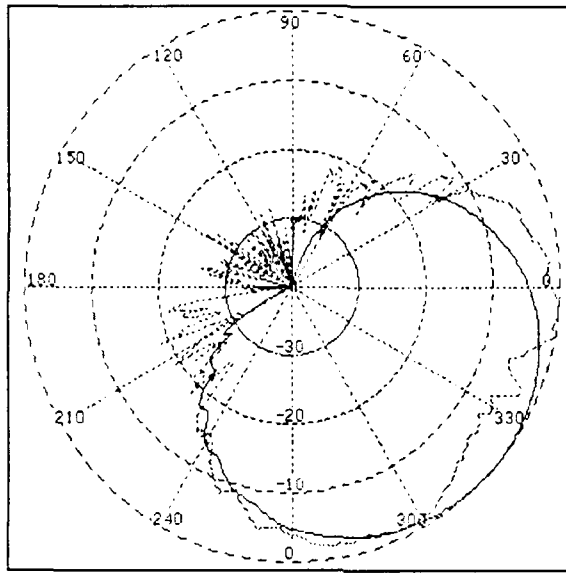
Figure 40.   FB-111A and Spiral An-
tenna Model at 15.0 GHz,
0° Elevation Predicted
(Solid Line) and Mea-
sured (Dotted Line)

5. __Effects of Varying Aircraft Model Dimensions__. The model was robust
to variations in aircraft model dimensions. Model configurations tested
were with no wings, wings swept to 46°, antenna relocated 5 inches
forward, and cross-sectional fuselage ellipsoid dimensions increased by
5 inches in each direction. The results show remarkably little vari-
ation in the model output for changes in the wing and fuselage geometry.

a. __Results Without Wings__. Figure 42 shows the model results with
the aircraft wings removed beyond the wing root. The figure shows the
absence of the very small effect of the diffraction from the wings.
This illustrates the small effect of the wing on the overall radiation
pattern since the wing edges are located far from the antenna and are
shadowed by the wing roots wherever antenna gain is appreciable.

72

(a) −20° Elevation   (b) −10° Elevation

(c) +10° Elevation   (d) +20° Elevation
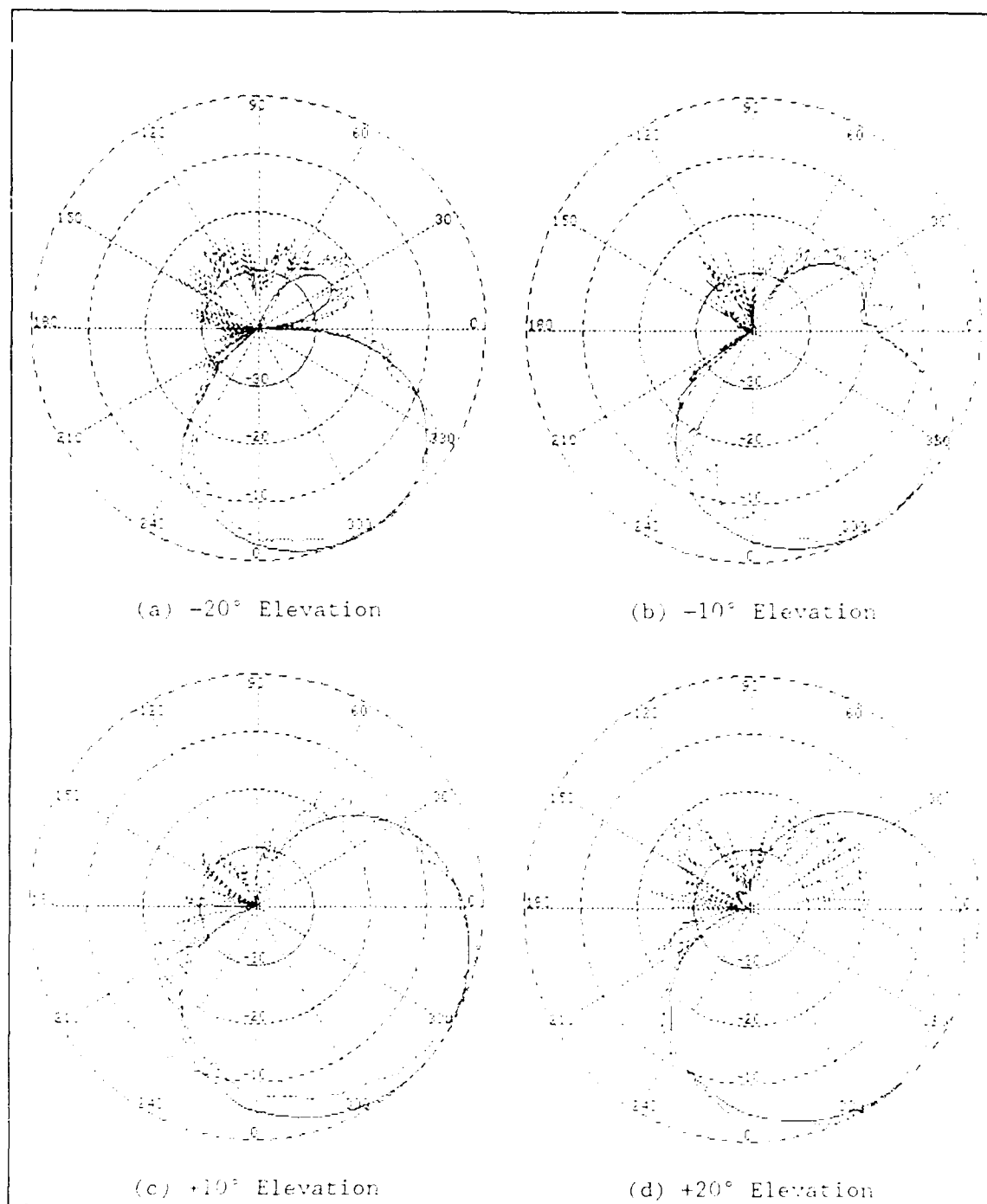
Figure 41. FB-111A Antenna Pattern at 15.0 GHz: Measured (Dotted Line) and Predicted (Solid Line)

(a) −20° Elevation   (b) +10° Elevation
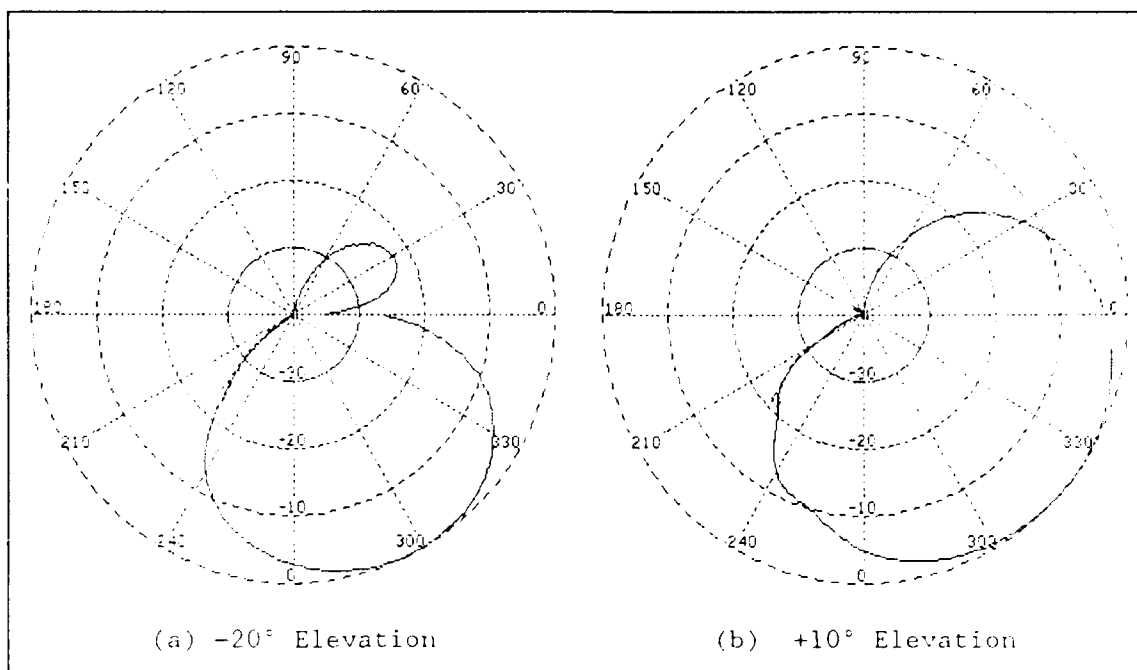
Figure 42. FB-111A with Spiral Antenna at 6.5 GHz, Without Wings (Solid Line) and With Wings (Dotted Line)

b. **Wings Swept to 46°**. Figure 43 shows the model results for a modified (46°) and original (40°) wing sweep. A slight shift in the angular location of the shadowing of the wing and wing root is apparent in the figure. There were no observable differences in the model results for positive elevation angles.

c. **Variation in Antenna Location**. Figure 44 shows the results of altering the antenna location on the aircraft, moving it 5 inches closer to the nose. The effect of incorrectly locating the antenna is negligible in the model results.

d. **Variations in Model Ellipsoid Dimensions**. Figure 45 shows the slightly more noticeable effects of specifying incorrect dimensions for the cross-sectional ellipse modeling the aircraft fuselage. The

(a) -20° Elevation   (b) -10° Elevation
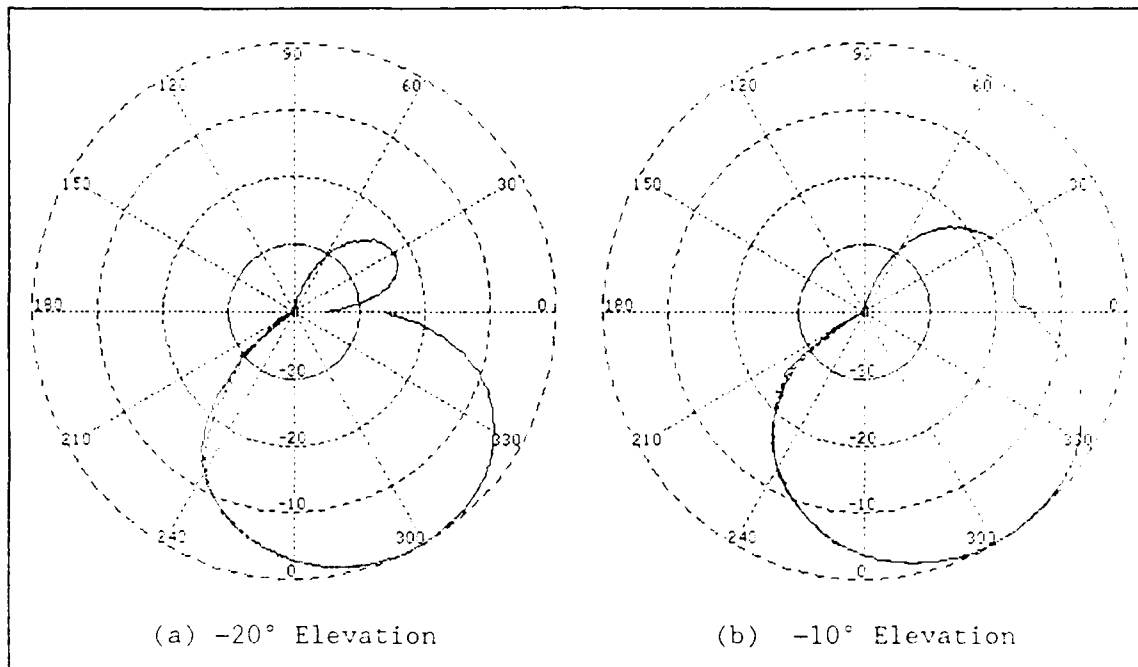
Figure 43.   FB-111A with Spiral Antenna at 6.5 GHz, Modeled With 46°
             Wing Sweep (Solid Line) and With 40° Wing Sweep (Dotted
             Line)

figure shows the results of overestimating the height and width dimen-
sion of the ellipsoid by 5 inches. At -20° elevation, the model result
for the region around the nose indicates slightly more gain than actual-
ly observed. At -10° elevation, the model slightly overestimates the
gain at azimuths near the nose. While noticeable, the differences
caused by using erroneous fuselage curvature are smaller than expected.
The stability of the scattering model to variation in these dimensions
implies that useable results can be achieved with only fairly well
estimated aircraft dimensions. This indicates that antenna pattern
modeling could be done early in an aircraft design before exact dimen-
sions are fixed. It also implies that the model would provide useful

(a) -20° Elevation   (b) 10° Elevation
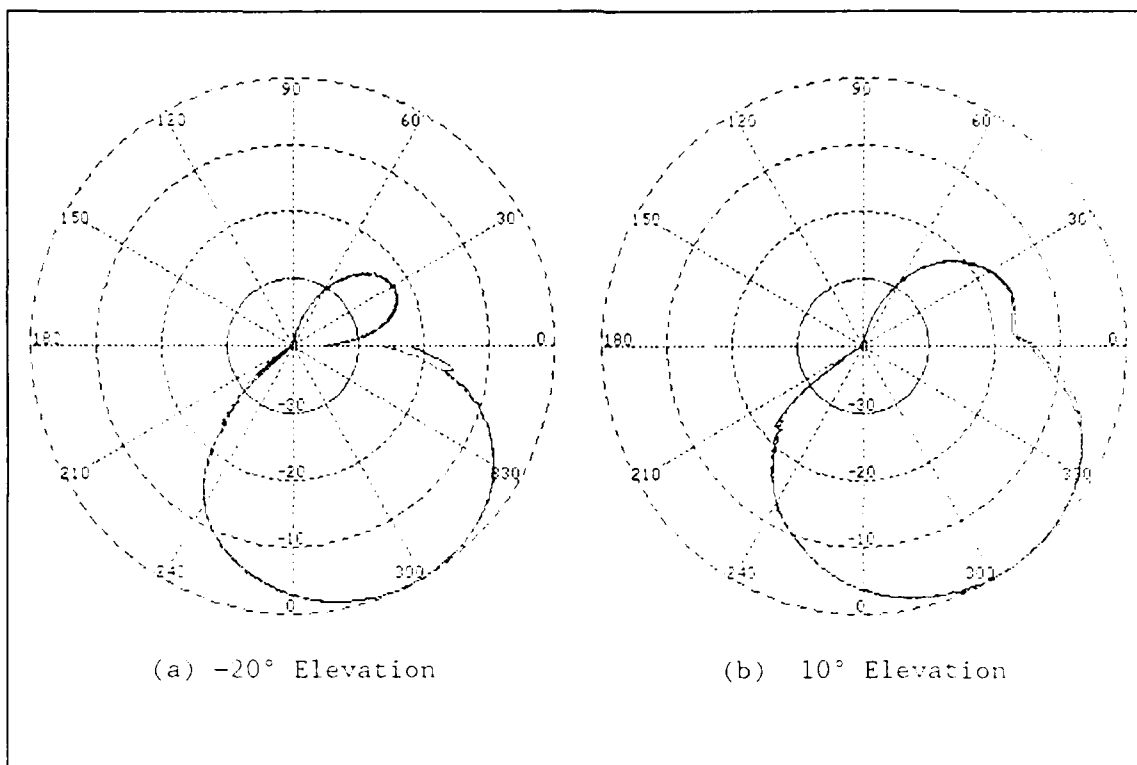
Figure 44. FB-111A with Spiral Antenna at 6.5 GHz, Modeled With Antenna
Shifted 5 inches Forward (Solid Line) and at Correct Antenna
Position (Dotted Line)

results for assessing enemy aircraft capabilities when only approximate

knowledge of the aircraft is available.

6. **Further Investigation of Antenna Pattern Phenomena**. This paragraph

includes selected results of attempts to isolate the causes of the

lobing evident in measured patterns for azimuths from 0° to 180°.

Eq (4) was used to determine the dimensions of a model plate that would

duplicate the observed lobing pattern at 6.5 GHz. The plate was added

to the model, and its position was adjusted until its effects reasonably

agreed with measured data. The scattering model was then run for all

elevation angles and two frequencies. Figure 46 and Figure 47 show the

(a) −20° Elevation　　　　　(b) 10° Elevation
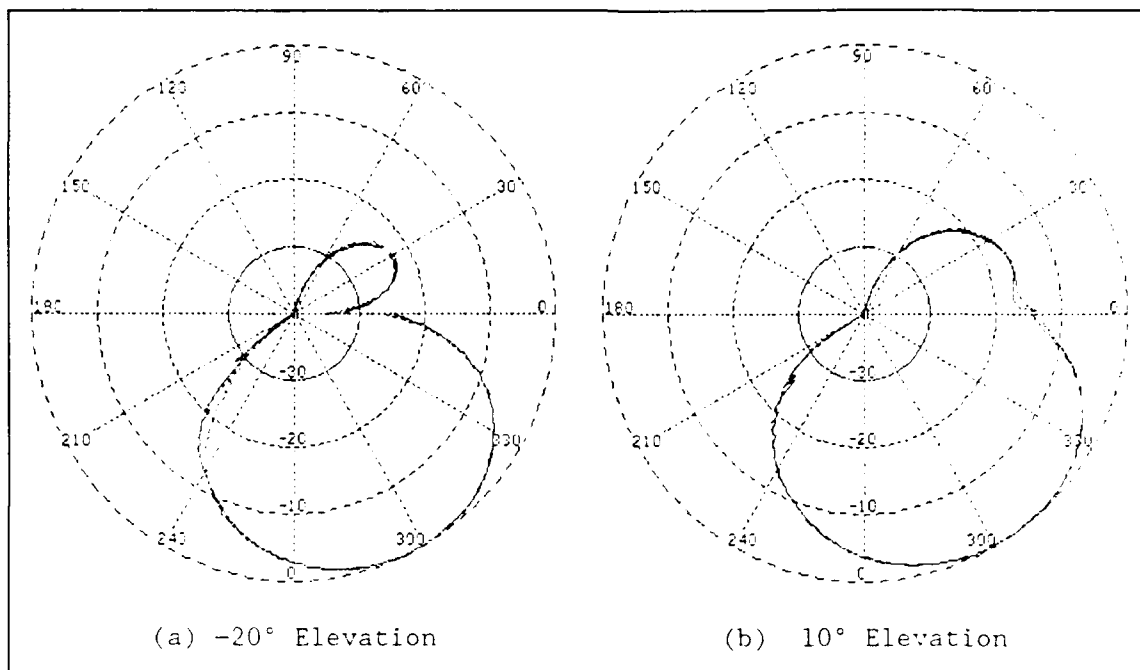
Figure 45. FB-111A with Spiral Antenna at 6.5 GHz, Modeled With Modi-
fied (Solid Line) and Actual (Dotted Line) Fuselage Curva-
ture

results at 6.5 GHz. Close agreement was achieved for +10° and +20°
elevation. At negative elevation angles the additional plate caused
noticeable attenuation in gain near 270° azimuth. Figure 48 and
Figure 49 show the results at 10.0 GHz. At 0° elevation, the additional
plate has some success modeling the reduction in gain at 270° azimuth,
but exaggerates the lobing present in the measured data from 0° to 90°
azimuth. At negative elevation angles, the additional plate severely
distorts the antenna pattern from 0° to 90° azimuth, and predicts much
less gain at 270° azimuth than was measured. While no additional model
plates could be derived to more closely duplicate the measurements over
all elevation angles and frequencies, the process of determining plate
sizes and experimenting with plate locations provided considerable
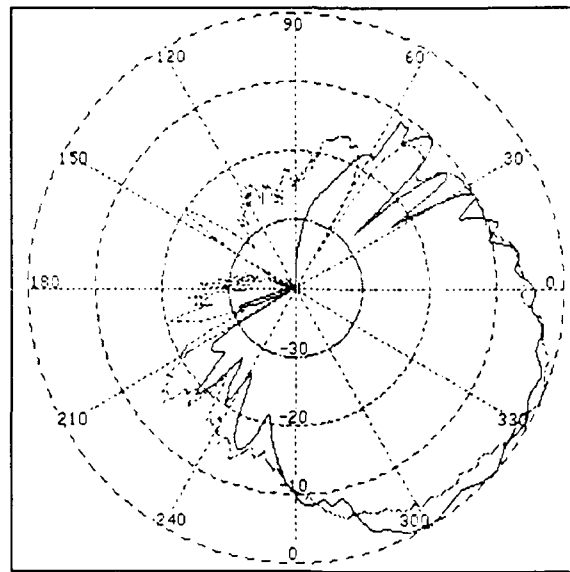
Figure 46. FB-111A and Spiral Antenna at 6.5 GHz, 0° Elevation, Modeled with Additional Model Plate (Solid Line) and Measured (Dotted Line)

insight on the effects aircraft components can have on antenna system performance. While not a particularly successful predictive tool, adding empirically derived plates to the model can facilitate analyzing the causes of observed phenomena. Once the causes of unpredicted scattering phenomena are hypothesized, other modeling methods can be applied to account for them. The UTD model can then become the basis of a more complete scattering model that accurately accounts for all scattering phenomenology. Once sufficient accuracy and detail are achieved, the complete model can be used to extrapolate known measured results.

(a) −20° Elevation   (b) −10° Elevation

(c) +10° Elevation   (d) +20° Elevation
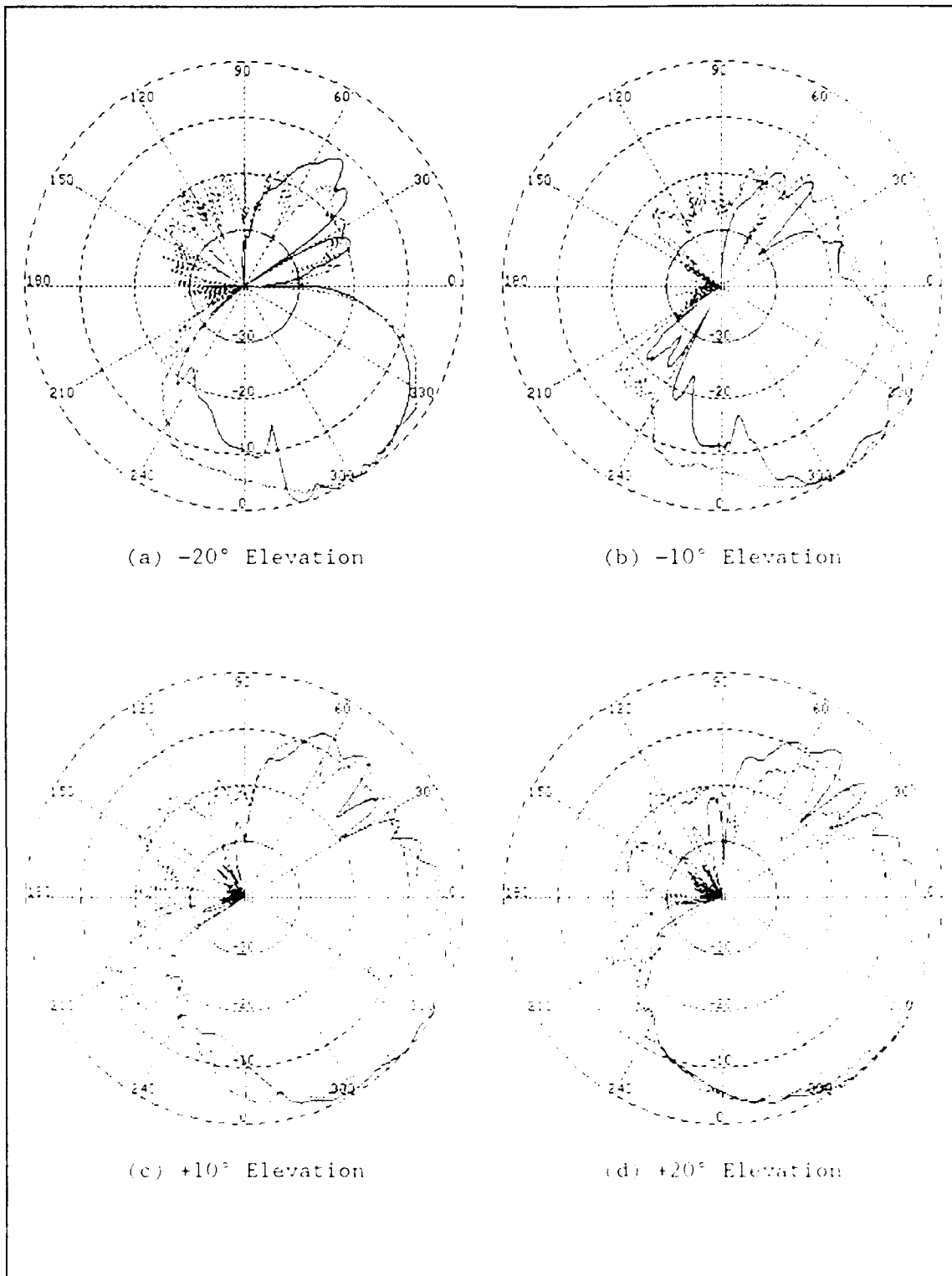
Figure 47. FB-111A Antenna Pattern at 6.5 GHz: Measured (Dotted Line) and Predicted (Solid Line) Using Additional Model Plate
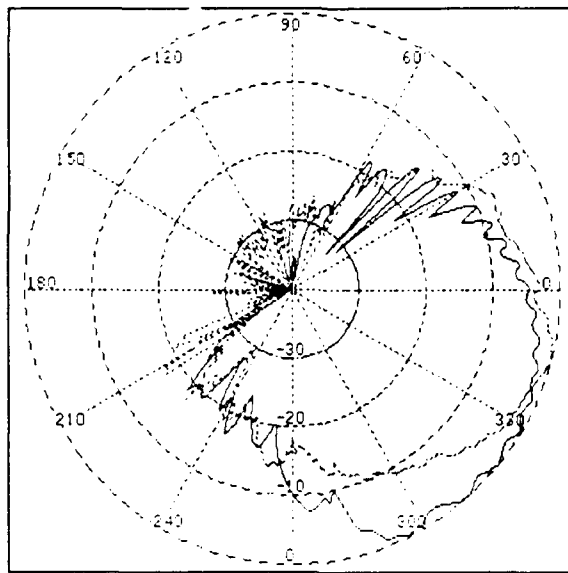
Figure 48. FB-111A and Spiral An-
tenna at 10.0 GHz, 0°
Elevation, Modeled with
Additional Model Plate
(Solid Line) and Mea-
sured (Dotted Line)

7. **Discussion of Results**.

a. **General Observations**. In general, the UTD model using the
spiral antenna and FB-111A models predicted the overall performance of
the antenna system under study, but failed to predict the un-modeled ef-
fects of the fuselage surface discontinuities. The shape of the pre-
dicted antenna patterns varied very little with frequency and model
dimensions. At all frequencies, there was a general tendency to overes-
timate the system gain around 0° and 270° azimuths. Measured gain in
the backlobe region as high as -10 dB. was absent from the model results

(a) -20° Elevation

(b) -10° Elevation

(c) +10° Elevation

(d) +20° Elevation
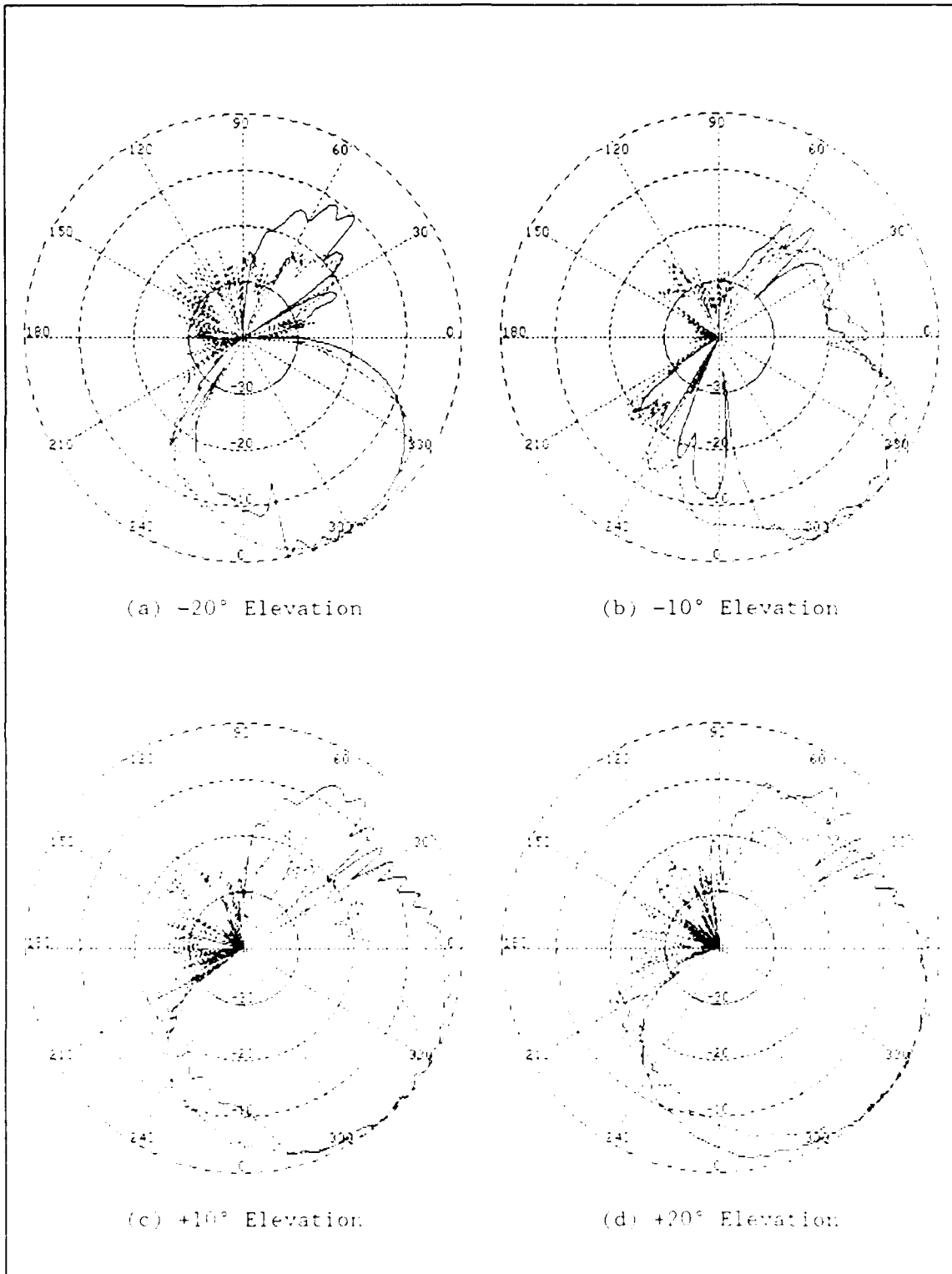
Figure 49. FB-111A Antenna Pattern at 10.0 GHz: Measured (Dotted Line) and Predicted (Solid Line) Using Additional Model Plate

due either to non-modeled effects of fuselage surface discontinuities in the main lobe region of the antenna or interaction between the antenna and the mounting surface. At positive elevation angles, the model failed to predict significant (as high as 15 dB) reduction in gain for azimuths around the nose at certain frequencies.

b. <u>Discussion of Differences Between Predicted and Observed Radiation Patterns</u>.

1) One notable difference observed between the model predictions and measured data was the previously-documented (Chung and Burnside, 1984:855-858) effect of the finite conductivity of the cockpit windscreen which, in this installation, was within three feet of the antenna. Diffraction caused by the abrupt change in conductivity at the fuselage-to-cockpit interface could also have significantly influenced the radiation pattern over the nose region. No accurate method of including the diffraction effects of this interface using UTD scattering shapes was found during this study.

2) The radiation pattern in the backlobe region of the antenna was not accurately predicted. The relatively high gain in the backlobe region would not be as apparent in the radiation pattern for an omnidirectional antenna installed at the same location, since even the highest gain (-10 dB, at 2.5 GHz) would be only a small ripple in the omnidirectional pattern around unity gain.

3) There was a trend in the model to overestimate the gain of the antenna system around 270° azimuth. The basic geometry of the aircraft does not suggest a mechanism for the measured reduction in gain

(of about 6 to 8 dB) in this region. Access panel drawings of the FB-111A and examination of a photograph of the measured system suggest the possibility of diffractions from surface gaps between fuselage access panels at this azimuth.

V Conclusions and Recommendations

1. **General**. The Airborne Antenna Radiation Pattern Code is a powerful tool for predicting basic characteristics of the principal-plane radiation patterns of cavity-backed spiral antennas mounted on the surface of an aircraft fuselage. The real strength of the code is the capability it provides in investigating the causes of known features in measured antenna radiation patterns. By providing the capability to vary parameters in the aircraft model to duplicate measured patterns in model predictions, the program provides an analyst or engineer insight on the causes of key features or problems in the measured pattern. By iterating the model with different aircraft model properties, the antenna system designer can experimentally determine the effects of changes in antenna location and aircraft con ˜uration without the expense of repeating radiation pattern measurements until a final design is selected.

2. **Specific Conclusions**.

    a. Using a nine-element monopole array model of the antenna, the Airborne Antenna Radiation Pattern Code can predict the general charac-teristics and shape of the radiation pattern of a cavity-backed spiral antenna mounted on a curved fuselage.

b. Experimentation with the geometric aircraft model provides valuable insight into the physical causes of observed radiation patterns.

c. Modeling the scattering from the basic aircraft shape is insufficient to fully characterize the radiation pattern of a directional antenna mounted on a fuselage surface. A fully successful antenna pattern model must also include the effects the fuselage surface features have on the antenna's performance.

3. **Recommendations**.

a. Recommend additional research in modeling the horizontal polarization characteristics of the cavity-backed spiral antenna using the Airborne Antenna Radiation Pattern Code.

b. Recommend investigation of combining the Airborne Antenna Radiation Pattern Code results with results of modeling fuselage plate joints using Method of Moments or wire grid models to improve predictions of the antenna system's performance in the backlobe region.

c. Recommend use of the Airborne Antenna Radiation Pattern Code by individuals involved in designing and testing cavity-backed spiral antenna installations. The code offers considerable flexibility in investigating the causes of unexpected radiation pattern characteristics through manipulation of the aircraft model.

d. Recommend use of the Airborne Antenna Radiation Pattern Code by individuals responsible for predicting or analyzing the probable

performance of cavity-backed spiral antennas installed on aircraft. Predicted results with a suitable aircraft model show the general shape of the actual antenna pattern. The prediction accuracy should provide useful engineering data for assessment of the capabilities of the airborne system using the antenna. However, the model tends to overestimate gain somewhat within 90° azimuth of the antenna boresight and ignore some mechanisms causing significant loss in gain at certain azimuths and elevations where near unity gain would be intuitively expected. The model's output should be interpreted as an optimistic prediction of the performance a system, and not as a guarantee of a given radiation pattern characteristic.

NEWAIR3.FOR Input File:

```
UN: Units are Inches
3
FQ: Frequency is 6 5 GHz
1,6.5000000,6.5000000
BO: Binary Output Desired
T
SG: Source Geometry Specified
-6.2000,.0000
9
.4361,90.0000
.9085,7.2683,.0000,.4543,3
.5000,86.4000
.0000,.0000
.9085,7.2683,.0000,.4543,3
1.0000,.0000
.4361,270.0000
.9085,7.2683,.0000,.4543,3
.5000,-86.4000
.6167,135.0000
.9085,7.2683,.0000,.4543,3
.2500,8.0000
.4361,180.0000
.9085,7.2683,.0000,.4543,3
.5000,-78.4000
.6167,225.0000
.9085,7.2683,.0000,.4543,3
.2500,-164.8000
.6167,45.0000
.9085,7.2683,.0000,.4543,3
.2500,164.8000
.4361,.0000
.9085,7.2683,.0000,.4543,3
.5000,78.4000
.6167,315.0000
.9085,7.2683,.0000,.4543,3
.2500,-8.0000
FG: Fuselage Curvature
29.5,36.9,200.3,184.5
F
0.,0.,0.
FC: Fuselage Chop
F,F
0.0,-34.0
PG: Plate 1 (Port Upper Wing Glove)
3
T
9.5,35.0,-23.0
```

```
-0.5,100.0,166.0
17.5,20.0,51.0
PG: Plate 2 (Starboard Upper Wing Glove)
3
T
17.5,-20.0,51.0
-0.5,-100.0,166.0
9.5,-35.0,-23.0
PG: Plate 3 (Port Wing)
4
F
-0.5,100.0,166.0
-5.5,367.3,376.0
-5.5,352.0,410.24
-0.818,70.0,284.591
PG: Plate 4 (Starboard Wing)
4
F
-0.818,-70.0,284.591
-5.5,-352.0,410.24
-5.5,-367.3,376.0
-0.5,-100.0,166.0
PG: Plate 5 (Port Fuselage Top)
6
T
17.5,20.0,51.0
-0.5,100.0,166.0
0.0,70.0,276.0
-8.163,70.0,476.0
3.480,0.0,476.0
21.031,0.0,46.0
PG: Plate 6 (Starboard Fuselage Top)
6
T
21.031,0.0,46.0
3.480,0.0,476.0
-8.163,-70.0,476.0
0.0,-70.0,276.0
-0.5,-100.0,166.0
17.5,-20.0,51.0
PG: Plate 7 (Port Vertical Stabilizer)
4
F
5.0,0.5,554.0
119.5,0.5,578.8
117.5,0.5,491.0
-15.5,0.5,324.0
PG: Plate 8 (Starboard Vertical Stabilizer)
4
F
-15.5,-0.5,324.0
119.5,-0.5,491.0
119.5,-0.5,578.7
```

```
5.0,-0.5,554.0
PG: Plate 9 (Leading Edge of Vertical Stabilizer)
4
F
-15.5,0.5,324.0
119.5,0.5,491.0
119.5,-0.5,491.0
-15.5,-0.5,324.0
PG: Plate 10 (Underside Fuselage Blockage)
4
F
-30.0,-80.0,0.0
-15.0,-80.0,476.0
-15.0,80.0,476.0
-30.0,80.0,0.0
FB: (Transparent Fuselage)
2
6
-28.8,0.0,-40.0
28.8,0.0,-40.0
29.5,0.0,0.0
28.9,0.0,40.0
-28.9,0.0,40.0
-29.5,0.0,0.0
6
0.0,-36.9,0.0
0.0,-32.2,90.0
0.0,-7.65,180.0
0.0,7.65,180.0
0.0,32.2,90.0
0.0,36.9,0.0
PD:
90.0,0.0,70.0
0,360,1
T,10000.
EX:
PD:
90.0,0.0,80.0
0,360,1
T,10000.
EX:
PD:
90.0,0.0,90.0
0,360,1
T,10000.
EX:
PD:
90.0,0.0,100.0
0,360,1
T,10000.
EX:
PD:
90.0,0.0,110.0
```

```
.
.

.

        0,360,1
        T,10000.
        EX:
```

NEWAIR3.FOR Output File:

```
*UN:                                                                         *
*    ALL FOLLOWING INPUT DATA GIVEN IN TERMS OF INCHES                        *
*FQ:                                                                          *
*    THE FOLLOWING FREQUENCY DIMENSIONS ARE IN GIGAHERTZ:                     *
*          NFREQ=   1   FREQI=      6.500   DFREQ=      6.500                  *
*BO:                                                                          *
*SG:                                                                          *
*    THERE ARE    9 SOURCES IN THIS COMPUTATION.                              *
*    PHASE CENTER IS PHS=   -6.20 DEGREES  ZS=      0.000  INCHES             *
*                                          LOCATION        EXCITATION         *
*SOURCE    TYPE     BETA     LENGTH      RHO      PHI       MAG      PHASE*
*------    ----   -------  ----------  -----------------  ---------------*
*  1      MONO     ---       0.45       0.44    90.00     0.50      86.40*
*  2      MONO     ---       0.45       0.00     0.00     1.00       0.00*
*  3      MONO     ---       0.45       0.44   270.00     0.50     -86.40*
*  4      MONO     ---       0.45       0.62   135.00     0.25       8.00*
*  5      MONO     ---       0.45       0.44   180.00     0.50     -78.40*
*  6      MONO     ---       0.45       0.62   225.00     0.25    -164.80*
*  7      MONO     ---       0.45       0.62    45.00     0.25     164.80*
*  8      MONO     ---       0.45       0.44     0.00     0.50      78.40*
*  9      MONO     ---       0.45       0.62   315.00     0.25      -8.00*
*FG: Fuselage Curvature                                                       *
*ELLIPSOID MODEL HAS THE FOLLOWING DIMENSIONS IN INCHES:                      *
*          A=  29.500,  B=  36.900,  C= 200.300,  D= 184.500                  *
*THE PATTERN ORIGIN LOCATION IS GIVEN BY THE FOLLOWING DIMENSIONS:            *
*          X=      0.000,  Y=      0.000,  Z=      0.000                       *
*FC:                                                                          *
*    THE FUSELAGE WILL BE CHOPPED OFF IN                                      *
*    ZC2=   -34.000  INCHES                                                   *
*PG: Plate 1 (Port Upper Wing Glove)                                          *
*    PLATE# 1 IS ADDED TO THIS SIMULATION MODEL                               *
*    PLATE# 1 IS ATTACHED TO FUSELAGE BY PROGRAM                              *
*PLATE#  CORNER#   INPUT LOCATION IN INCHES    ACTUAL LOCATION IN METERS *
*------  -------  --------------------------  -------------------------- *
*   1       1       9.500,  35.000, -23.000     0.241,   0.889,  -0.584 *
*   1       2      -0.500, 100.000, 166.000    -0.013,   2.540,   4.216 *
*   1       3      17.500,  20.000,  51.000     0.444,   0.508,   1.295 *
*PG: Plate 2 (Starboard Upper Wing Glove)                                     *
*    PLATE# 2 IS ADDED TO THIS SIMULATION MODEL                               *
*    PLATE# 2 IS ATTACHED TO FUSELAGE BY PROGRAM                              *
*PLATE#  CORNER#   INPUT LOCATION IN INCHES    ACTUAL LOCATION IN METERS *
*------  -------  --------------------------  -------------------------- *
*   2       1      17.500, -20.000,  51.000     0.444,  -0.508,   1.295 *
*   2       2      -0.500,-100.000, 166.000    -0.013,  -2.540,   4.216 *
*   2       3       9.500, -35.000, -23.000     0.241,  -0.889,  -0.584 *
*PG: Plate 3 (Port Wing)                                                      *
*    PLATE# 3 IS ADDED TO THIS SIMULATION MODEL                               *
*PLATE#  CORNER#   INPUT LOCATION IN INCHES    ACTUAL LOCATION IN METERS *
*------  -------  --------------------------  -------------------------- *
*   3       1      -0.500, 100.000, 166.000    -0.013,   2.540,   4.216 *
*   3       2      -5.500, 367.300, 376.000    -0.140,   9.329,   9.550 *
```

91

```
*    3        3        -5.500, 352.000, 410.240     -0.140,   8.941,  10.420 *
*    3        4        -0.818,  70.000, 284.591     -0.021,   1.778,   7.229 *
*PG: Plate 4 (Starboard Wing)                                               *
*    PLATE# 4 IS ADDED TO THIS SIMULATION MODEL                             *
*PLATE#   CORNER#   INPUT LOCATION IN INCHES    ACTUAL LOCATION IN METERS *
*------   -------   ------------------------    ------------------------- *
*    4        1        -0.818, -70.000, 284.591     -0.021,  -1.778,   7.229 *
*    4        2        -5.500,-352.000, 410.240     -0.140,  -8.941,  10.420 *
*    4        3        -5.500,-367.300, 376.000     -0.140,  -9.329,   9.550 *
*    4        4        -0.500,-100.000, 166.000     -0.013,  -2.540,   4.216 *
*PG: Plate 5 (Port Fuselage Top)                                            *
*    PLATE# 5 IS ADDED TO THIS SIMULATION MODEL                             *
*    PLATE# 5 IS ATTACHED TO FUSELAGE BY PROGRAM                            *
*PLATE#   CORNER#   INPUT LOCATION IN INCHES    ACTUAL LOCATION IN METERS *
*------   -------   ------------------------    ------------------------- *
*    5        1        17.500,  20.000,  51.000      0.444,   0.508,   1.295 *
*    5        2        -0.500,  00.000, 166.000     -0.013,   2.540,   4.216 *
*    5        3         0.000,  70.000, 276.000      0.000,   1.778,   7.010 *
*    5        4        -8.163,  70.000, 476.000     -0.207,   1.778,  12.090 *
*    5        5         3.480,   0.000, 476.000      0.088,   0.000,  12.090 *
*    5        6        21.031,   0.000,  46.000      0.534,   0.000,   1.168 *
*PG: Plate 6 (Starboard Fuselage Top)                                       *
*    PLATE# 6 IS ADDED TO THIS SIMULATION MODEL                             *
*    PLATE# 6 IS ATTACHED TO FUSELAGE BY PROGRAM                            *
*PLATE#   CORNER#   INPUT LOCATION IN INCHES    ACTUAL LOCATION IN METERS *
*------   -------   ------------------------    ------------------------- *
*    6        1        21.031,   0.000,  46.000      0.534,   0.000,   1.168 *
*    6        2         3.480,   0.000, 476.000      0.088,   0.000,  12.090 *
*    6        3        -8.163, -70.000, 476.000     -0.207,  -1.778,  12.090 *
*    6        4         0.000, -70.000, 276.000      0.000,  -1.778,   7.010 *
*    6        5        -0.500,-100.000, 166.000     -0.013,  -2.540,   4.216 *
*    6        6        17.500, -20.000,  51.000      0.444,  -0.508,   1.295 *
*PG: Plate 7 (Port Vertical Stabilizer)                                     *
*    PLATE# 7 IS ADDED TO THIS SIMULATION MODEL                             *
*PLATE#   CORNER#   INPUT LOCATION IN INCHES    ACTUAL LOCATION IN METERS *
*------   -------   ------------------------    ------------------------- *
*    7        1         5.000,   0.500, 554.000      0.127,   0.013,  14.072 *
*    7        2       119.500,   0.500, 578.800      3.035,   0.013,  14.702 *
*    7        3       117.500,   0.500, 491.000      2.984,   0.013,  12.471 *
*    7        4       -15.500,   0.500, 324.000     -0.394,   0.013,   8.230 *
*PG: Plate 8 (Starboard Vertical Stabilizer)                                *
*    PLATE# 8 IS ADDED TO THIS SIMULATION MODEL                             *
*PLATE#   CORNER#   INPUT LOCATION IN INCHES    ACTUAL LOCATION IN METERS *
*------   -------   ------------------------    ------------------------- *
*    8        1       -15.500,  -0.500, 324.000     -0.394,  -0.013,   8.230 *
*    8        2       119.500,  -0.500, 491.000      3.035,  -0.013,  12.471 *
*    8        3       119.500,  -0.500, 578.700      3.035,  -0.013,  14.699 *
*    8        4         5.000,  -0.500, 554.000      0.127,  -0.013,  14.072 *
*PG: Plate 9 (Leading Edge of Vertical Stabilizer)                          *
*    PLATE# 9 IS ADDED TO THIS SIMULATION MODEL                             *
*PLATE#   CORNER#   INPUT LOCATION IN INCHES    ACTUAL LOCATION IN METERS *
*------   -------   ------------------------    ------------------------- *
*    9        1       -15.500,   0.500, 324.000     -0.394,   0.013,   8.230 *
```

```
*    9        2     119.500,    0.500, 491.000      3.035,    0.013,  12.471 *
*    9        3     119.500,   -0.500, 491.000      3.035,   -0.013,  12.471 *
*    9        4     -15.500,   -0.500, 324.000     -0.394,   -0.013,   8.230 *
*PG: Plate 10 (Underside Fuselage Blockage)                                 *
*    PLATE#10 IS ADDED TO THIS SIMULATION MODEL                             *
*PLATE#  CORNER#    INPUT LOCATION IN INCHES      ACTUAL LOCATION IN METERS *
*------  -------    ------------------------      ------------------------- *
*   10        1     -30.000,  -80.000,   0.000     -0.762,   -2.032,   0.000 *
*   10        2     -15.000,  -80.000, 476.000     -0.381,   -2.032,  12.090 *
*   10        3     -15.000,   80.000, 476.000     -0.381,    2.032,  12.090 *
*   10        4     -30.000,   80.000,   0.000     -0.762,    2.032,   0.000 *
*FB: (Transparent Fuselage?)                                                *
*    THERE ARE    2  PLATES TO SIMULATE THE' FUSELAGE BLOCKAGE              *
*PLATE#  CORNER#    INPUT LOCATION IN INCHES      ACTUAL LOCATION IN METERS *
*------  -------    ------------------------      ------------------------- *
*    1        1     -28.800,    0.000, -40.000     -0.732,    0.000,  -1.016 *
*    1        2      28.800,    0.000, -40.000      0.732,    0.000,  -1.016 *
*    1        3      29.500,    0.000,   0.000      0.749,    0.000,   0.000 *
*    1        4      28.900,    0.000,  40.000      0.734,    0.000,   1.016 *
*    1        5     -28.900,    0.000,  40.000     -0.734,    0.000,   1.016 *
*    1        6     -29.500,    0.000,   0.000     -0.749,    0.000,   0.000 *
*    2        1       0.000,  -36.900,   0.000      0.000,   -0.937,   0.000 *
*    2        2       0.000,  -32.200,  90.000      0.000,   -0.818,   2.286 *
*    2        3       0.000,   -7.650, 180.000      0.000,   -0.194,   4.572 *
*    2        4       0.000,    7.650, 180.000      0.000,    0.194,   4.572 *
*    2        5       0.000,   32.200,  90.000      0.000,    0.818,   2.286 *
*    2        6       0.000,   36.900,   0.000      0.000,    0.937,   0.000 *
*PG: Plate 11 (Axial Fuselage Discontinuity)                               *
*    PLATE#11 IS ADDED TO THIS SIMULATION MODEL                            *
*    PLATE#11 IS ATTACHED TO FUSELAGE BY PROGRAM                           *
*PLATE#  CORNER#    INPUT LOCATION IN INCHES      ACTUAL LOCATION IN METERS *
*------  -------    ------------------------      ------------------------- *
*   11        1      27.800,  -12.000,  -?.000      0.706,   -0.305,  -0.051 *
*   11        2      29.900,  -12.350,  -8.000      0.759,   -0.314,  -0.203 *
*   11        3      27.800,  -12.000,  -8.000      0.706,   -0.305,  -0.203 *
*PD:                                                                        *
*    PATTERN AXIS DEFINED BY: 90.00,   0.00  CONICAL PATTERN ANGLE=  70.00*
*    THE RANGE OF PATTERN ANGLES FOR THIS RUN IS:   0,360, 1              *
*    THIS IS FAR FIELD PATTERN !!!                                          *
*EX:                                                                        *
*****************************************************************************
* DIMENSIONS OF THE CROSS-SECTION AT THE PHASE CENTER IN TERMS OF INCHES
29.50000        36.90000
* PHI VALUE OF THE SOURCE ORIENTATION AT THE PHASE CENTER:
-4.0 DEGREES
* AX,BX,CX,DX,ZS,VRS,VES,VESP:
 0.7493000        0.9372600        5.087620        4.686300        0.0000000E+00
-8.6631544E-02   0.0000000E+00   0.0000000E+00
*ELLIPSOID DIMENSIONS USED IN GEODESIC CALCULATION:AF,BF,CF,AFP,BFP,CFP,
ZSHIFT
 0.7493000        0.9372600        5.087620        0.7493000        0.9372600
4.686300         0.0000000E+00
* ELEVATION PLANE CAUSTIC ANGLE: CBTRR,CBTRL
```

```
 -0.3658399      -0.3812535
* PLATE ATTACHMENT TO THE FUSELAGE: MP,DL1,DL2
        1    1.304592       0.5078774
        2   0.5078774       1.304592
        5   0.4872642      -0.3702718
        6  -0.3702718       0.4872642
       11   3.3493865E-02  1.1865381E-02
```

Bibliography

Balanis, Constantine A. *Advanced Engineering Electromagnetics*. New York: John Wiley and Sons, 1989.

---- *Antenna Theory Analysis and Design*. NewYork: John Wiley and Sons, 1982.

---- and Dennis DeCarlo. "Monopole Antenna Patterns on Finite Size Composite Ground Planes," IEEE Transactions on Antennas and Propagation, 30; 764–768 (July 1982).

Baron, Allan R. and others. "Passive Direction Finding and Signal Location," *Microwave Journal, 25*: 59–76+ (September 1982).

Burnside, Walter D. and Ronald J. Marhefka. *Antenna Handbook: Theory, Applications, and Design*. Yuen T. Lo and Shung-Wu Lee (editors). New York: Van Nostrand Reinhold Company, 1988.

Burnside, Walter D. and others. *Airborne Antenna Radiation Pattern Code User's Manual*. Report Number 716199-4. The Ohio State University ElectroScience Laboratory, September 1985.

---- and others. "Near-Field Pattern Analysis of Airborne Antennas," *IEEE Transactions on Antennas and Propagation, 28*: 318–327 (May 1980).

---- and others. "Roll-Plane Analysis of On-Aircraft Antennas," *IEEE Transactions on Antennas and Propagation*, 21: 780–786 (November 1973).

Chung, H. H. and Walter D. Burnside. "Analysis of Airborne Antenna Radiation Patterns Using Spheroid/Plates Model," *Proceedings of the IEEE International Symposium on Antennas and Propagation*. 855–858. New York: IEEE Press, 1984.

Cooke, William P. and Charles E. Ryan, Jr. "A Geometrical Theory of Diffrac-·tion Computer Algorithm for Computing the Radiation Patterns of Aircraft-Mounted Antennas," *Proceedings of the IEEE International Symposium on Antennas and Propagation*. 631–634. New York: IEEE Press (1980).

Department of the Air Force. *Organizational Maintenance General Aircraft Information*. T.C. 1F-111(B)A-2-1 Change 38. Sacramento: Sacramento Air Logistics Center, 30 October 1989.

Fahmy, Mostapha N. I. and Adel Z. Botros. "Radiation from Quarter Wavelength Monopoles on Finite Cylindrical, Conical, and Rocket-Shaped Conducting Bodies," *IEEE Transactions on Antennas and Propagation,* 27: 615- 624 (September 1979).

Howell, N. Alleyne. "Calculation of Antenna Pattern with an Obstruction in the Near Field," *Proceedings of the IEEE International Symposium on Antennas and Propagation.* 46-49. New York: IEEE Press (1975).

Keller, James B. "Geometrical Theory of Diffraction," *Journal of the Optical Society of America,* 52:116-130 (February 1962).

Kim, Jacob J. and Walter D. Burnside. "Simulation and Analysis of Antennas Radiating in a Complex Environment," *IEEE Transactions on Antennas and Propagation,* 34: 554-562 (April 1986).

Kline, Morris and Irvin W. Kay. *Electromagnetic Theory and Geometric Optics.* New York: Interscience Publishers (1985).

Kouyoumjian, Robert G. and Prabhakar H. Pathak. "A Uniform Geometrical Theory of Diffraction for an Edge in a Perfectly-Conducting Surface." *Proceedings of the IEEE.* 1448-1461. New York: IEEE Press (1974)

Kraus, John D. "Antennas: Our Electronic Eyes and Ears," *Electronic Warfare Design Engineers' Handbook.* Norwood, MA: Horizon House-Microwave (1990).

----- *Electromagnetics.* New York: McGraw-Hill (1984).

Marhefka, Ronald J. and Walter D. Burnside. *Numerical Electromagnetic Code-Basic Scattering Code User's Manual.* Report Number 712242-14. The Ohio State University ElectroScience Laboratory, July 1983.

----- and Walter D. Burnside. "Analysis of Wing Mounted Antenna Patterns," *IEEE Transactions on Antennas and Propagation.* 24:562-565 (June 1976).

----- and Walter D. Burnside. "Analysis of Wing Mounted Antenna Pat- terns," *IEEE Transactions on Antennas and Propagation,* 24:562-565 (June 1976).

Miller, Jay. *General Dynamics F-111 "Aardvark".* Fallbrook, CA: Aero Publishers (1982)

Pathak, Prabhakar H. *Antenna Handbook: Theory, Applications, and Design.* Yuen T. Lo and Shung-Wu Lee (editors). New York: Van Nostrand Reinhold Company, 1988.

----- and others. "A Uniform GTD Solution for the Radiation from Sources on a Convex Surface, " *IEEE Transactions on Antennas and Propagation,* 29: 609-622 (July 1981).

Pedrotti, Frank L. and Leno S. Pedrotti. *Introduction to Optics.* Englewood Cliffs, NJ: Prentice-Hall, 1987.

Rome Air Development Center. *FB-111 ALR-74 and ASPJ Antenna Pattern Measurements*. Report Number RBCC-84-052-1. Rome, New York: (1984).

Rome Air Development Center. *FB-111 ALR-74 Antennas in Nose Radome, Behind Canopy and Casting Swap Measurements*. Report Number RBCC-84-053-1. Rome, New York: (1984).

Rome Air Development Center. *Rome Air Development Center Antenna Pattern Standard Magnetic Tape Format Description*. Report Number RBCC-82-23-1. Rome, New York (1984).

Salas, Saturnino L. and Einar Hille. *Calculus, One and Several Variables*. New York: John Wiley and Sons (1974).

Skolnik, Merrill I. *Introduction to Radar Systems*. New York: McGraw Hill, 1980.

Tsui, James Bao-Yen. *Microwave Receivers with Electronic Warfare Applications*. New York: John Wiley and Sons, 1986.

Veruttipong, Thavath W. "Computer Simulation Technique for the Determination of the Best Location of Airborne Antennas," *Proceedings of the IEEE Region 5 Conference*. 35-38. New York: IEEE Press, 1984.

Yu, Chong L. and others. "Volumetric Pattern Analysis of Airborne Antennas," *IEEE Transactions on Antennas and Propagation, 26:* 636-641 (September 1978).

---- and Walter D. Burnside. "Analysis of Fuselage Mounted-Antenna Patterns," *Proceedings of IEEE International Symposium on Antennas and Propagation*. 558-561. New York: IEEE Press, 1976.

Vita

Captain David P. Carroll was born on 13 February 1949 in San Bernardino, California. He graduated from Aquinas High School in San Bernardino in 1967 and enlisted in active duty in the U. S. Air Force in September, 1967. While enlisted, Captain Carroll worked in cryptographic and record communications maintenance, attaining Master Sergeant rank. He was selected for the Airman Education and Commissioning Program and attended Auburn University, Alabama, graduating with a Bachelor of Science in Electrical Engineering in August, 1981. Upon commissioning via Officer Training School in December 1981, Captain Carroll was assigned to the Air Force Electronic Warfare Center, San Antonio, Texas. There he developed models for radar warning receiver emitter identification algorithms and participated in several major evaluations of electronic warfare systems and electronic combat exercises. In June 1985, Captain Carroll was assigned to the Joint Intelligence Center, Stuttgart-Vaihingen, Germany. There he was chief of the signals analysis division, supervising a multi-million dollar upgrade to its signal parameter measurement laboratory. While at Stuttgart, Captain Carroll obtained a Master of Science in Systems Management from the University of Southern California. Captain Carroll entered the School of Engineering, Air Force Institute of Technology, in May 1989.

Permanent Address: 1122 Stevenson Street

Colton, California

REPORT DOCUMENTATION PAGE

1. AGENCY USE ONLY *(Leave blank)*	2. REPORT DATE December 1990	3. REPORT TYPE AND DATES COVERED Master's Thesis

4. TITLE AND SUBTITLE Predicting the Performance of Airborne Antennas in the Microwave Regime	5. FUNDING NUMBERS
6. AUTHOR(S) David P. Carroll, Captain, USAF	

7. PERFORMING ORGANIZATION NAME(S) AND ADDRESS(ES) Air Force Institute of Technology, WPAFB, Ohio 45433-6583	8. PERFORMING ORGANIZATION REPORT NUMBER AFIT/GE/ENG/90D-10

9. SPONSORING/MONITORING AGENCY NAME(S) AND ADDRESS(ES)	10. SPONSORING/MONITORING AGENCY REPORT NUMBER

11. SUPPLEMENTARY NOTES

12a. DISTRIBUTION/AVAILABILITY STATEMENT Approved for Public Release; Distribution Unlimited	12b. DISTRIBUTION CODE

13. ABSTRACT *(Maximum 200 words)*

This study investigated the application of a high-frequency model (Uniform Geometrical Theory of Diffraction) of electromagnetic sources mounted on a curved surface of a complex structure. In particular, the purpose of the study was to determine if the model could be used to predict the radiation patterns of cavity-backed spiral antennas mounted on aircraft fuselages so that the optimum locations for the antennas could be chosen during the aircraft design phase. A review of literature revealed a good deal of work in modeling communications, navigation, identification antennas (blade monopoles and aperture slots) mounted on a wide variety of aircraft fuselages and successful validation against quarter-scale model measurements. This study developed a monopole-array model of a spiral antenna's radiation at vertical polarization and an ellipsoid-plate model of the FB-111A. Using the antenna and aircraft models, the existing Uniform Geometrical Theory of Diffraction model generated radiation patterns which agreed favorably with full-scale measured data. The study includes plots of predicted and measured radiation patterns from 2.5 to 15 Gigahertz.

14. SUBJECT TERMS Broadband Antennas; Radiation Patterns; Airborne Antennas; Microwave Antennas; Computer Modeling; Spiral Antennas	15. NUMBER OF PAGES 107
	16. PRICE CODE

17. SECURITY CLASSIFICATION OF REPORT Unclassified	18. SECURITY CLASSIFICATION OF THIS PAGE Unclassified	19. SECURITY CLASSIFICATION OF ABSTRACT Unclassified	20. LIMITATION OF ABSTRACT UL